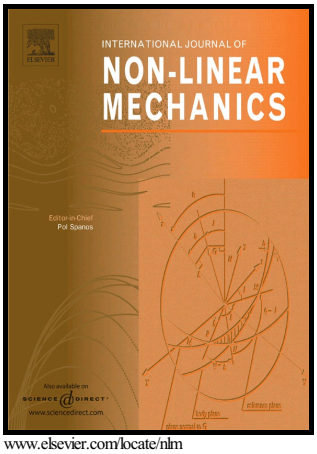

www.elsevier.com/locate/nlm

Asymptotic solutions for the Föppl – von Kármán equations governing deflections of thin axisymmetric annular plates

Robert A. Van Gorder

PII: S0020-7462(17)30085-9
DOI: http://dx.doi.org/10.1016/j.ijnonlinmec.2017.02.004
Reference: NLM2784

To appear in: *International Journal of Non-Linear Mechanics*

Cite this article as: Robert A. Van Gorder, Asymptotic solutions for the Föppl – von Kármán equations governing deflections of thin axisymmetric annular plates *International Journal of Non-Linear Mechanics* http://dx.doi.org/10.1016/j.ijnonlinmec.2017.02.004

Asymptotic solutions for the Föppl – von Kármán equations governing deflections of thin axisymmetric annular plates

Robert A. Van Gorder
Mathematical Institute, University of Oxford, Andrew Wiles Building, Radcliffe Observatory Quarter, Woodstock Road, Oxford, OX2 6GG, United Kingdom

Robert.VanGorder@maths.ox.ac.uk

Abstract
We are concerned with the deformation of thin, flat annular plates under a force applied orthogonally to the plane of the plate. This mechanical process can be described via a radial formulation of the Föppl – von Kármán equations, a set of nonlinear partial differential equations describing the deflections of thin flat plates. We are able to obtain analytical solutions for the radial Föppl – von Kármán equations with boundary conditions relevant for clamped, loosely clamped, and free inner and outer. This permits us to study the qualitative behavior of the out-of-plane deflections as well as the Airy stress function for a number of cases. Provided that an appropriate non-dimensionalization is taken, we find that the perturbation solutions are surprisingly valid for a wide variety of parameters, and compare favorably with numerical simulations in all cases (rather than just for small parameters). The results demonstrate that the ratio of the inner to outer radius of the annular plate will strongly influence the properties of the solutions, as will the specific boundary data considered. For instance, one may choose to fix the plate in place with a specific set of boundary conditions, in order to minimize the out-of-plane deflections. Other boundary conditions may result in undesirable behaviors.

Keywords: Föppl – von Kármán equations; deflections of thin flat plates; nonlinear PDEs; analytical solution

1. Introduction

The Föppl – von Kármán equations, a set of nonlinear partial differential equations describing the large deflections of thin flat plates, read

$$D\nabla^4 w - h\left(\frac{\partial^2 F}{\partial y^2}\frac{\partial^2 w}{\partial x^2}+\frac{\partial^2 F}{\partial x^2}\frac{\partial^2 w}{\partial y^2}-2\frac{\partial^2 F}{\partial x\partial y}\frac{\partial^2 w}{\partial x\partial y}\right)=P(x,y), \tag{1a}$$

$$\nabla^4 F + E\left\{\frac{\partial^2 w}{\partial x^2}\frac{\partial^2 w}{\partial y^2}-\left(\frac{\partial^2 w}{\partial x\partial y}\right)^2\right\}=0, \tag{1b}$$

where $w=w(x,y)$ is the out of plane deflection, $F=F(x,y)$ is the Airy stress function, E is Young's modulus, h is the thickness of the plate,

$$D=\frac{Eh^3}{12\left(1-\nu^2\right)}$$

is called the flexural (or, cylindrical rigidity, or, bending stiffness, in various literature) of the plate, ν is Poisson's ratio, and $P(x,y)$ is the external normal force per unit area of the plate.

Furthermore, $\nabla^4 = \Delta^2$ denotes the biharmonic operator

$$\nabla^4 = \frac{\partial^4}{\partial x^4} + \frac{\partial^4}{\partial y^4} + 2\frac{\partial^4}{\partial x^2 \partial y^2}.$$

There is a long history to these equations (see, e.g., [1-4]). There is a dynamic form of the Föppl - von Kármán equations,

$$h\rho \frac{\partial^2 w}{\partial t^2} + D\nabla^4 w - h\left(\frac{\partial^2 F}{\partial y^2}\frac{\partial^2 w}{\partial x^2} + \frac{\partial^2 F}{\partial x^2}\frac{\partial^2 w}{\partial y^2} - 2\frac{\partial^2 F}{\partial x \partial y}\frac{\partial^2 w}{\partial x \partial y} \right) = P(x,y), \tag{2a}$$

$$\nabla^4 F + E\left\{ \frac{\partial^2 w}{\partial x^2}\frac{\partial^2 w}{\partial y^2} - \left(\frac{\partial^2 w}{\partial x \partial y} \right)^2 \right\} = 0, \tag{2b}$$

which govern, for instance, vibrations of thin plates [5-8]. This formulation has also been used to study vibrations of axially symmetric shells [9]. Note that the time-dependent formulation (2) can be used to solve the static equations (1) numerically, as solutions to (1) would be steady state solutions to (2); see [10]. While the numerical and experimental study of these equations has been well represented in the literature, few analytical results have been reported. Chen and Hutchenson [11] and Huang, Hong and Suo [12] recently conducted analysis on the equations, under certain specific assumptions and special cases. Regarding the buckling of the plate, Audoly [13] performs a weakly-nonlinear analysis above the buckling threshold, and the results are compared to numerical simulations. Analytical solutions in the case of the straight-sided blister governing by the Föppl – von Kármán equations are given in [14-16]. Mathematically, such results correspond to an infinite strip with a sinusoidal profile. Further results in the form of sinusoidal functions are given for the herringbone pattern in [17,18]. From a purely mathematical point, the Föppl – von Kármán equations have been studied by Knightly in [19], who established a priori estimates and a global existence theorem, and furthermore showed that for small data the solution is unique.

Due to the fact that the Föppl – von Kármán equations involve high order derivatives, along with two types of nonlinearities [20], numerical solutions are typically obtained, as the problem is often too challenging for analytical methods. However, the Föppl – von Kármán equations describe the large deformations of a plate, and hence are of interest to those studying deformations and wrinkling of surfaces [21-25] or even blistering of such surfaces [26]. For these reasons, a method of obtaining approximate analytical solutions is of interest. An analytical method for the Föppl – von Kármán equations was considered in [27], where the optimal homotopy analysis method was applied to obtain approximate analytical solutions in the case of clamped boundary conditions for rectangular plates.

While most studies on the Föppl – von Kármán equations have been for either rectangular or circular plates, it is possible to consider more general structures. Let us consider a flat plate taking the shape of the connected domain Ω in the plane. In order to solve the Föppl – von Kármán equations, we need to impose boundary conditions, and these are determined by the particular application at hand. Regarding standard boundary condition for the Föppl – von Kármán equations, the loosely clamped edge boundary conditions [28] read

$$w = \frac{\partial^2 w}{\partial \mathbf{n}^2} = 0 \quad \text{and} \quad F = \frac{\partial^2 F}{\partial \mathbf{n}^2} = 0 \quad \text{for} \quad (x,y) \in \partial\Omega, \tag{3}$$

where $\mathbf{n}$ is the outward normal vector to the boundary $\partial\Omega$. Meanwhile, the clamped edge

boundary conditions [28] read

$$w = \frac{\partial w}{\partial \mathbf{n}} = 0 \quad \text{and} \quad F = \frac{\partial^2 F}{\partial \mathbf{n}^2} = 0 \quad \text{for } (x, y) \in \partial\Omega, \tag{4}$$

with the difference here being that $\frac{\partial w}{\partial \mathbf{n}} = 0$ rather than $\frac{\partial^2 w}{\partial \mathbf{n}^2} = 0$ is taken on the boundary $\partial\Omega$. Finally, if a boundary is not affixed to anything, but rather hangs free, one may consider the free boundary conditions

$$\frac{\partial^2 w}{\partial \mathbf{n}^2} = \frac{\partial^3 w}{\partial \mathbf{n}^3} = 0 \quad \text{and} \quad F = \frac{\partial F}{\partial \mathbf{n}} = 0 \quad \text{for } (x, y) \in \partial\Omega, \tag{5}$$

as discussed in [29]. There exists some analytical theory dealing with plate theory under mixed boundary conditions; see [30]. We shall focus on various pairings of boundary conditions (3)-(5), as these are the conditions which arise commonly in the literature for various kinds of flat plates.

In addition to references mentioned above, there has been particular interest in plates with a circular geometry. In contrast to the fourth-order Föppl – von Kármán equations, the second order von Kármán equations have been considered in [31-36], where various analytical results for the deflection of circular plates were given. A more detailed derivation of the constitutive equations governing the stresses in circular flat plates is provided in [37]. In early work on annular plates was carried out by Evans and Hart [38,39]. They considered theoretical results, and compared the von Kármán results with corresponding results for the Reissner formulation. Additional work on the annular plate theory under the von Kármán model was considered in [40-42]. More mathematically rigorous existence and uniqueness results for annular plate problems were presented in [43,44].

The study of annular plates or membranes is relevant to applications involving the ponding of annular membranes [45], corona geometry gel swelling [23,46], optical membranes relating to space-based inflatable technology [47], and the flowering cabbage plants or the growth of plant leaves [48]. When temporal effects are considered, the vibrations of annular membranes have also been studied [49-51]. Temporal terms also allow one to couple the plate dynamics to thermal field, in order to study the influence of heat transfer on the bending process; see [52]. The Föppl – von Kármán equations have been considered in order to describe annular sheets at a molecular level, with monoatomic graphene sheets having been studied in [53]. While this study will be concerned with annular plates having radial symmetry, we remark that annular plates with deflections varying both with the radial variable and with the angular variable have been considered, and are studied in order to better understand the process of wrinkling [54-56]. Deformations of a axisymmetric thin, circular stiff membrane resting on an elastic foundation have been studied analytically and numerically [57], and such results have relevance to tissue engineering. Finally, the annular plate model may be seen as a local approximation for the stress and displacement locally around a point fixing embedding in a plate composed of glass [58,59] or metal [60,61]. Despite the interest in solving the Föppl – von Kármán equations and various simplifications, we note that the thin deflections of an annular plate have not been considered analytically under this model. Furthermore, although sheets with point fixings often involve single sheets with more than on hole, no analytical results are found in the literature, and hence consideration of the annular sheet is a relevant first step.

Motivated by the variety of applications for which the bending of annular flat plates could prove useful, this paper is devoted to the study of solutions to the Föppl – von Kármán equations (1) for annular flat plates under various physically relevant boundary conditions,

namely those given in (3)-(5), with a focus on demonstrating that some pairings of these conditions give fairly natural results, while other pairings give results which are not useful or physical. Asymptotic solutions are desirable, as they grant us a qualitative understanding of the out-of-plane deformations, and for all cases considered we shall provide analytical approximations. Numerical simulations are then used to verify the results, and we show that the analytical solutions remain valid even for larger values of the magnitude of deformation of the plate. For mathematical tractability, we shall assume that the bending of the plates will be axisymmetric (as is commonly done in the literature), which is valid for constant or strictly radial forcing. This permits us to study a mathematically tractable problem.

The paper is organized as follows. In Section 2, we outline the general mathematical problem for the thin annular plate under the Föppl – von Kármán equations. In Section 3, we consider annular plates with clamped or loosely clamped inner edge condition and free outer edge condition, and this is relevant to situations where the disk is held fixed at the center yet is left free out the outer edge - such as what we see when point fixings are used. In Section 4, we consider the reverse: The outer edge is clamped or loosely clamped, while the inner edge is held free. We show that these plates are more poorly behaved than their counterparts studied in other sections. In Section 5, we consider various combinations orfclamped or loosely clamped inner *and* outer edges, and for this case the results are all qualitatively similar. We discuss the results and offer concluding remarks in Section 6.

2. Föppl – von Kármán equations for a thin annular plate

In this section, we now formulate the relevant mathematical problem for a thin flat sheet taking the form of an axisymmetric annulus, with a central hole and a larger outer radius. For sake of analytical tractability, and to employ the Föppl – von Kármán equations, we shall consider a flat annular disc of uniform thickness, of outer radius L and inner radius $\tilde{\varepsilon} > 0$ located at the center of the disc. See Figure 1 for the problem geometry.

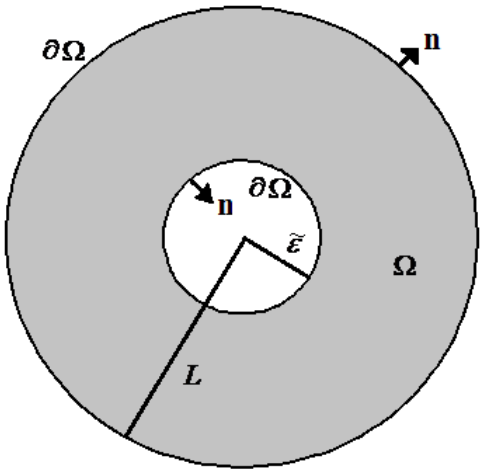

Figure 1: Geometry of the problem.

We will first attempt to study the nonlinear equations using a perturbation approach, which will be made possible by considering small amplitude deflections of the annular plate under the assumption of radial symmetry. Later, we shall also consider numerical solutions. We

shall begin by considering the radial problem in non-dimensional form. To this end, we introduce a non-dimensional solution of the form

$$w(x,y)=\frac{Lh\delta}{\sqrt{12\left(1-\sigma^2\right)}}u(r),\quad F(x,y)=\frac{ELh^2\delta}{12\left(1-\sigma^2\right)}f(r),\quad P(x,y)=\frac{L^5h^5\delta}{\left[12\left(1-\sigma^2\right)\right]^{3/2}}\hat{P}(r), \tag{6}$$

where $r=L^{-1}\sqrt{x^2+y^2}$ is the non-dimensional length in the radial direction while $\delta>0$ is a small non-dimensional parameter which we take to be of the order of the deflection of the plate. Under the Föppl – von Kármán formulation, it makes physical sense to consider $\delta\ll Lh$. In this way, the displacement function $u(r)$ can be taken as order one, $O(1)$, in the parameter δ. In the non-dimensional model, the outer radius of the plate is one, while the inner radius of the plate is $\varepsilon=\tilde{\varepsilon}L^{-1}$ so that $0<\varepsilon<1$. The system (1) then becomes

$$\frac{1}{r}\frac{d}{dr}\left(r\frac{d}{dr}\left[\frac{1}{r}\frac{d}{dr}\left(r\frac{du}{dr}\right)\right]\right)=\frac{d^4u}{dr^4}+\frac{2}{r}\frac{d^3u}{dr^3}-\frac{1}{r^2}\frac{d^2u}{dr^2}+\frac{1}{r^3}\frac{du}{dr}=\frac{\delta}{r}\frac{d}{dr}\left(\frac{df}{dr}\frac{du}{dr}\right)+\hat{P}(r), \tag{7a}$$

$$\frac{1}{r}\frac{d}{dr}\left(r\frac{d}{dr}\left[\frac{1}{r}\frac{d}{dr}\left(r\frac{df}{dr}\right)\right]\right)=\frac{d^4f}{dr^4}+\frac{2}{r}\frac{d^3f}{dr^3}-\frac{1}{r^2}\frac{d^2f}{dr^2}+\frac{1}{r^3}\frac{df}{dr}=-\frac{\delta}{r}\frac{du}{dr}\frac{d^2u}{dr^2}. \tag{7b}$$

Consider an annular plate hanging by a clamp or loose clamp at the interior radius. At the boundary $r=1$, we will take free boundary conditions for the moment. The relevant boundary conditions at $r=\varepsilon$ will depend upon properties of the point fixing. If the point fixing is a loose clamp at $r=\varepsilon$, then we should have the conditions

$$u(\varepsilon)=u''(\varepsilon)=f(\varepsilon)=f''(\varepsilon)=0, \tag{8a}$$

$$u''(1)=u'''(1)=f(1)=f'(1)=0. \tag{8b}$$

On the other hand, if the point fixing acts as a clamp at $r=\varepsilon$, we have the slightly modified boundary conditions

$$u(\varepsilon)=u'(\varepsilon)=f(\varepsilon)=f''(\varepsilon)=0, \tag{9a}$$

$$u''(1)=u'''(1)=f(1)=f'(1)=0. \tag{9b}$$

Here we have replaced the condition $u''(\varepsilon)=0$ in (8a) with the condition $u'(\varepsilon)=0$ in (9a).

If we are interested in the problem of an annular plate suspended at the outer edge by a clamp or loose clamp while the inner edge hangs free, we solve the same problem (7), only with the boundary conditions reversed. Note that it is also possible to consider annular plates with clamped or loosely clamped conditions at each of the two boundaries as well.

Since solutions will differ in qualitative structure for each set of boundary conditions, in Section 3 we consider solutions under the fixed clamp boundary conditions (8) and loose clamp boundary conditions (9) at the inner edge of the annular plate, with free boundary conditions on the outer edge. In both cases, analytical approximations are give in order to study each problem qualitatively, while numerical solutions are given in order to verify the accuracy of the analytical results.

3. Clamped or loosely clamped condition on the inner edge of the plate, free conditions on the outer edge

We first consider situations where the annular plate is clamped or loosely clamped on the inner edge, and left free on the outer edge. This is the configuration most common when a plate is held in place by a centrally located point fixing.

3.1. The annular plate with loosely clamped inner edge conditions

We solve (7) subject to the loosely clamped boundary conditions (8). We shall consider the case where $\delta > 0$ is a small perturbation parameter, meaning that deflections of the plate are sufficiently small. If we assume a solution which scales like

$$u(r) = u_0(r) + \delta u_1(r) + O(\delta^2), \quad f(r) = f_0(r) + \delta f_1(r) + O(\delta^2), \tag{10}$$

then we obtain

$$\frac{1}{r}\frac{d}{dr}\left(r\frac{d}{dr}\left[\frac{1}{r}\frac{d}{dr}\left(r\frac{du_0}{dr}\right)\right]\right) = \hat{P}(r), \tag{11a}$$

$$\frac{1}{r}\frac{d}{dr}\left(r\frac{d}{dr}\left[\frac{1}{r}\frac{d}{dr}\left(r\frac{df_0}{dr}\right)\right]\right) = 0, \tag{11b}$$

$$\frac{1}{r}\frac{d}{dr}\left(r\frac{d}{dr}\left[\frac{1}{r}\frac{d}{dr}\left(r\frac{du_1}{dr}\right)\right]\right) = \frac{1}{r}\frac{d}{dr}\left(\frac{df_0}{dr}\frac{du_0}{dr}\right), \tag{11c}$$

$$\frac{1}{r}\frac{d}{dr}\left(r\frac{d}{dr}\left[\frac{1}{r}\frac{d}{dr}\left(r\frac{df_1}{dr}\right)\right]\right) = -\frac{1}{r}\frac{du_0}{dr}\frac{d^2u_0}{dr^2}, \tag{11d}$$

and so on for higher order terms. In general, for an equation of the form

$$\frac{1}{r}\frac{d}{dr}\left(r\frac{d}{dr}\left[\frac{1}{r}\frac{d}{dr}\left(r\frac{dQ(r)}{dr}\right)\right]\right) = q(r), \tag{12}$$

the homogeneous solution will be

$$Q_{\text{hom}}(r) = \gamma_1 r^2 + \gamma_2 + \gamma_3 r^2 \ln(r) + \gamma_4 \ln(r), \tag{13}$$

whereas the particular solution will be

$$Q_{\text{part}}(r) = \int_0^r \frac{1}{r_4}\left\{\frac{1}{r_r}\int_0^{r_4}\left\{r_3\int_0^{r_3}\left\{\frac{1}{r_2}\int_0^{r_2} r_1 q(r_1)\,dr_1\right\}dr_2\right\}dr_3\right\}dr_4. \tag{14}$$

In each of the equations given in (11), the form of $q(r)$ will always be known, so the particular solution (14) can always be calculated. Solving (11a) using the relevant boundary conditions in (8), we obtain

$$u_0(r) = \gamma_1(\varepsilon) r^2 + \gamma_2(\varepsilon) + \gamma_3(\varepsilon) r^2 \ln(r) + \gamma_4(\varepsilon)\ln(r) + U_0(r), \tag{15}$$

where the particular solution $U_0(r)$ is given in terms of the force on the plate by the formula

$$U_0(r) = \int_0^r \frac{1}{r_4}\int_0^{r_4} r_3 \int_0^{r_3}\frac{1}{r_2}\int_0^{r_2} r_1 \hat{P}(r_1)\,dr_1 dr_2 dr_3 dr_4, \tag{16}$$

and the four constants $\gamma_k(\varepsilon)$ are derived in Appendix A and given in (A5)-(A8). One can construct higher order terms in the expansion (10) similarly.

Clearly, the solution will depend strongly on the value of the parameter ε governing the

size of the inner radius. In the limit where ε becomes negligibly small, note that the solution is still well-defined (the constants all remain finite since each term $\ln(\varepsilon)$ will always be multiplied by a term involving a positive power of ε), and we obtain

$$u_0(r) = \frac{3U_0'''(1) - 2U_0''(1)}{4} r^2 - U_0(0) - \frac{1}{2} U_0''(1) r^2 \ln(r) + U_0(r), \tag{17}$$

in the limit $\varepsilon \to 0$.

Next, solving (11b) along with the relevant boundary conditions (8), we obtain

$$f_0(r) = 0, \tag{18}$$

which makes sense due to the fact that (11b) has no forcing term. Yet, since $f_0(r) = 0$, equation (11c) has no forcing term and we obtain

$$u_1(r) = 0. \tag{19}$$

The inhomogeneity for equation (11d) depends on $u_0(r)$, which is non-zero as shown above, so the function $f_1(r)$ is non-zero as well. Plugging the solution (15) into (11d), we can obtain the closed form solution $f_1(r)$. This means that the out of plane deflection and the Airy stress functions scale as

$$w(x,y) = \delta u_0(r) + O(\delta^3) \text{ and } F(x,y) = \delta^2 f_1(r) + O(\delta^3), \tag{20}$$

respectively, for small δ. We omit the lengthy expression for $f_1(r)$, although we note that it will take a form similar to that given in equation (15).

In the special case where the force term is constant over the flat plate, say $\hat{P}(r) = p$, note that we obtain the specific functional form

$$U_0(r) = \frac{p}{64} r^4, \tag{21}$$

which we can then use in (15) and (A5)-(A8). We shall make use of this simplification later. More generally, if we prescribe a power-law force term, $\hat{P}(r) = pr^m$, for some power-law index $m \geq 0$ and some constant $p \in \mathbb{R}$, we will have

$$U_0(r) = \frac{p}{(m+2)^2 (m+4)^2} r^{m+4}. \tag{22}$$

For more complicated forms of the force term, the particular solution $U_0(r)$ cannot always be calculated in closed form (even for simple trigonometric functions). However, given a convergent Taylor series expansion for a specific choice of $\hat{P}(r)$, say

$$\hat{P}(r) = \sum_{m=0}^{\infty} p_m r^m, \tag{23}$$

we can calculate (from (22) and by the linearity of integral considered), that the particular solution $U_0(r)$ must take the form

$$U_0(r)=\sum_{m=0}^{\infty}\frac{p_m r^{m+4}}{(m+2)^2(m+4)^2}. \tag{24}$$

Note that the series (24) converges whenever the series (23) is convergent.

In the case of a constant force term $\hat{P}(r)=p$, we can plot the out of plane deflection and the Airy stress function. We give the out of plane deflection and the Airy stress function for various values of ε in Figure 2. The curves given for $\varepsilon=0$ correspond to the limit $\varepsilon\to 0^+$, which is well-defined anaytically. This limit corresponds to the point fixing of negligible radius, like those studied in the previous section. We see that the maximal deflection occurs at the free boundary ($r=1$). As a function of ε, the maximal displacement increases, attains a maximal value, and then decreases. The maximal stress occurs along a circle in the interior of the circular flat plate. Note that we plot $-f_1(r)$ in order to recover the magnitude of the Airy stress function, since $f_1(r)\le 0$ for this particular example. As expected, the stresses are orders of magnitude smaller than the deflections.

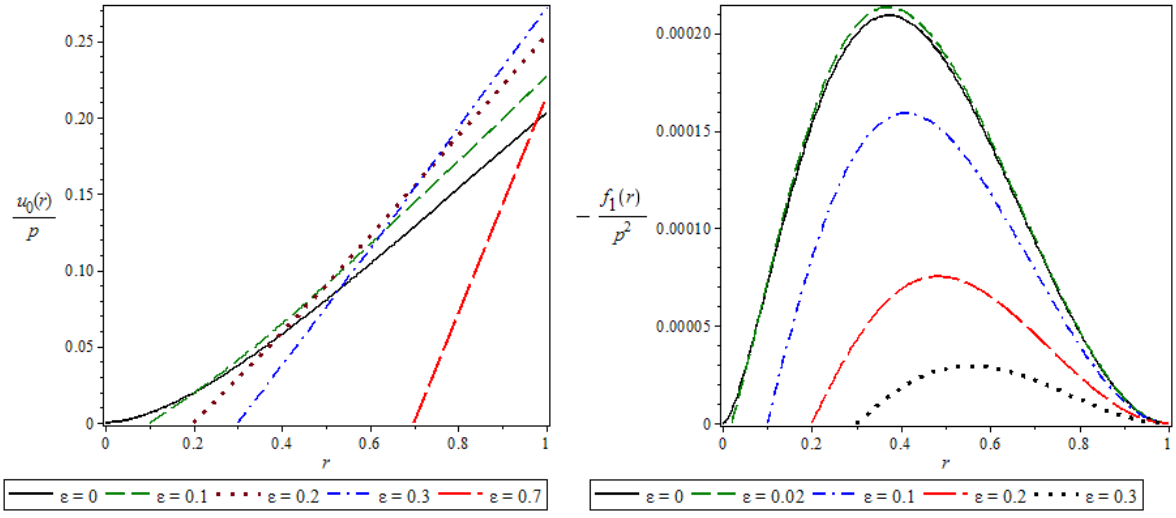

(a) (b)

Figure 2: Plot of (a) the first approximation $u_0(r)$ *in the expansion* $w(x,y)\sim\delta u_0(r)+O(\delta^3)$ *for the deflection of the annular flat plate and (b) the first approximation* $f_1(r)$ *in the expansion* $F(x,y)\sim\delta^2 f_1(r)+O(\delta^3)$ *for the Airy stress function on the annular flat plate, where* $\delta\ll 1$ *is a small parameter. Here the constant force term* p *is scaled out of the solutions in an appropriate way, and we have considered the loosely clamped boundary conditions as given in (8).*

For a constant force term $\hat{P}(r)=p$, we can plot the maximal deflection and the maximal value of the Airy stress function as functions dependent on ε. These results are shown in Figures 3. Note that both quantities are well-defined in the limit $\varepsilon\to 0^+$. The maximal displacement

always occurs at the free boundary, so $\max_{\varepsilon<r<1} \frac{u_0(r)}{p} = \frac{u_0(1)}{p}$. Over $0<\varepsilon<1$, we find that the largest deflection (of size $\max_{\varepsilon<r<1} \frac{u_0(r)}{p} = 0.2786456580$) occurs when $\varepsilon = 0.4018$, which is a fairly large inner radius compared to the size of the plate. Therefore, for rather small ε, say $0<\varepsilon \ll 1$, we notice an increasing trend in the displacement with an increase in the radius of the point fixing. As we take the point fixing radius to zero, we find that $\max_{\varepsilon<r<1} \frac{u_0(r)}{p} \to \frac{13}{64}$ as $\varepsilon \to 0^+$. The maximal stress occurs on the interior of the annular region, so for each fixed $0<\varepsilon<1$, we calculate $\max_{\varepsilon<r<1} \frac{|f_1(r)|}{p^2}$. For very small ε, there is an increasing trend in the maximal stress, before the stress function then quickly decreases in maximal magnitude as ε increases. The largest maximal value for the Airy stress function occurs for $\varepsilon \approx 0.02$.

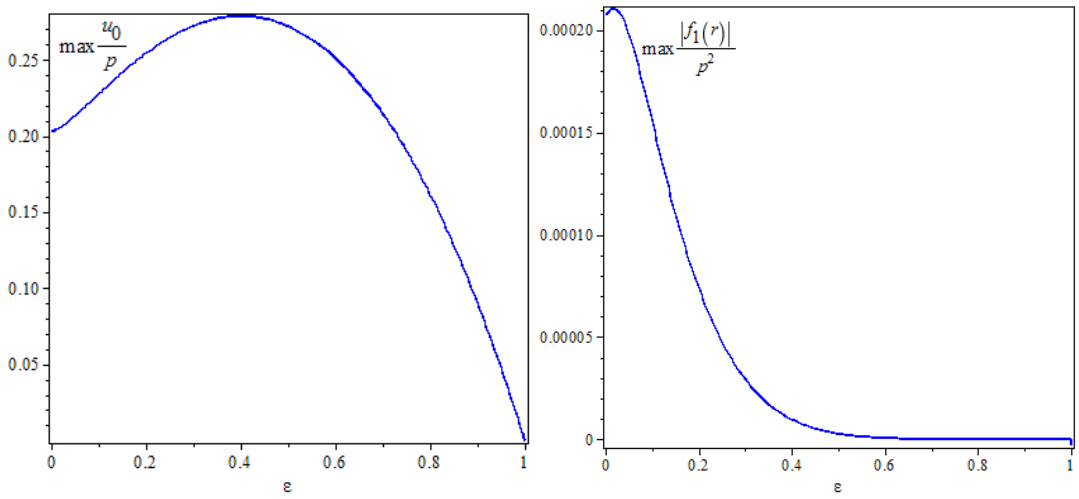

(a) (b)

Figure 3: Plot of (a) the scaled maximal displacement of the plate in the case of constant unifrom forcing, $\max_{\varepsilon<r<1} \frac{u_0(r)}{p} \sim \max_{\varepsilon^2<x^2+y^2<L^2} \frac{w(x,y)}{p\delta}$ *, and (b) the scaled maximal Airy stress function in the case of uniform forcing,* $\max_{\varepsilon<r<1} \frac{|f_1(r)|}{p^2} \approx \max_{\varepsilon^2<x^2+y^2<L^2} \frac{|F(x,y)|}{p^2\delta^2}$ *, as a function of the point fixing radius* $0<\varepsilon<1$*. We have considered the loosely clamped boundary conditions (8). Here the constant force term* p *is scaled out of the solution.*

In order to verify our perturbation results, we compare them with numerical simulations obtained using the boundary value problem solver in Maple. In Figure 4(a) we plot the scaled displacement of the plates for various values of the interior radius, while in Figure 4(b) we plot the Airy stress functions for each case. We find not only that the results are in excellent

agreement with the small δ regime, but also that the displacements do not vary over δ, even for large values of δ. This means that the scaling considered in (6) is indeed the natural scaling, and that the perturbation results remain physically relevant even for large values of δ. Hence, it is sufficient to understand the small-δ perturbation solution in order to understand the qualitative behavior of deflections to the annular plate.

For Figure 4(b), we choose the non-dimensional interior radius, ε, to be $\varepsilon = 0.3$, although similar results hold for other values. Note that a variety of scaling parameter sizes are considered, yet they do not appear to influence the structure of the solutions, only the magnitude of the solutions. Indeed, for each power of 10 increase in δ, we observe a power 10 increase in $f(r)$ (apart from at the boundaries, where the stresses tend rapidly to zero). What this suggests is that the scaling chosen in (6) could be adapted so that an additional factor of δ appears. Note that this is completely consistent with the perturbation result given in (20), which suggests that the Airy stress function actually scales like $F(x,y) \sim \delta^2 f_1(r) + O(\delta^3)$.

Both findings are completely consistent with the scalings we derived in (20). Since we have scaled out the relevant powers of δ in (20), we find that the first perturbation terms $u_0(r)$ and $f_1(r)$ hold the relevant qualitative data on the solutions. What this tells us is that one can treat the radial solutions as $w(x,y) = \delta u_0(r)$ and $F(x,y) = \delta^2 f_1(r)$, as higher-order terms are not essential (even for larger δ). Therefore, understanding $u_0(r)$ and $f_1(r)$ is sufficient for understanding the axisymmetric annular plate problem under the Föppl – von Kármán equations.

We should note that, as the interior radius is taken to zero, the numerical solutions begin to have problems for larger values of δ. For this limit, we actually have more confidence in the analytical results than the numerical simulations in the very small ε limit.

While we have preformed numerical simulations for all cases considered in this paper, the results will always agree with the perturbation results in that $u_0(r)$ and $f_1(r)$ are independent of the choice of δ for reasonable values of δ. In other words, the numerical results are in agreement with the analytical results for all cases considered. Therefore, we shall not reproduce numerical plots for each case, and instead we focus on the analytical results for the rest of this paper.

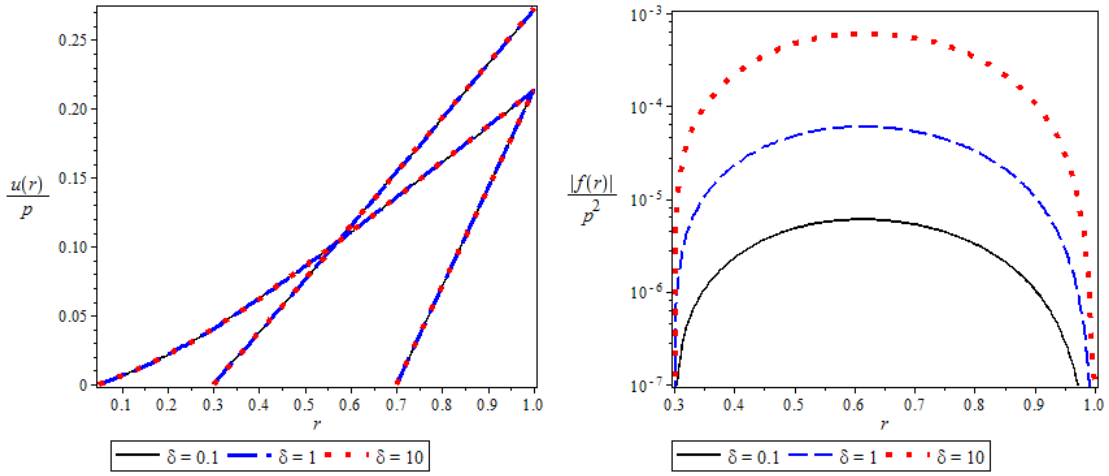

(a) (b)

Figure 4: Plot of the numerical solutions to (a) $u(r)$ *for the deflection of the annular flat plate and (b)* $f(r)$ *for the scaled Airy stress function obtained by solving (7) subject to loosely clamped boundary conditions (8) for various values of the scaling parameter* δ*. Here the constant force term* p *is scaled out of the solutions. Three choices of the non-dimensional interior radius,* ε*, are used for the deflections; namely,* $\varepsilon = 0.05$*,* $\varepsilon = 0.3$*, and* $\varepsilon = 0.7$*, although similar results hold for other values. Since the Airy stress function does depend on* δ*, we fix* $\varepsilon = 0.3$ *and focus on the variation with* δ*. If we were to have scaled* $f(r)$ *with an additional factor of* δ*, these stress curves would all be coincident.*

3.2. The annular plate with clamped inner edge conditions

We again consider the situation where $\delta > 0$ is a small perturbation parameter, and we solve (7) subject to the clamped boundary conditions (9). We assume the same perturbation solutions (10) and hence obtain the same governing equations. The only difference here is that we replace the boundary conditions (8) with the boundary conditions (9). Then, since we still have a general solution of the form (15), while $U_0(r)$ is still of the form given in (16), we obtain modified parameter values (given in Appendix A, equations (A13)-(A16)).

When a specific form of the forcing term is given, we can then uniquely determine the function $u_0(r)$ from (15). As we did in the previous subsection, for a constant force term $\hat{P}(r) = p$, we can plot the out of plane deflection and the Airy stress function, and we do so for various values of ε in Figure 5. The curves given for $\varepsilon = 0$ correspond to the limit $\varepsilon \to 0^+$, which is well-defined analytically. This limit corresponds to the point fixing of negligible radius, like those studied in the previous section. As we see, the maximal displacement occurs at the free boundary ($r = 1$). As a function of ε, the maximal displacement decreases.

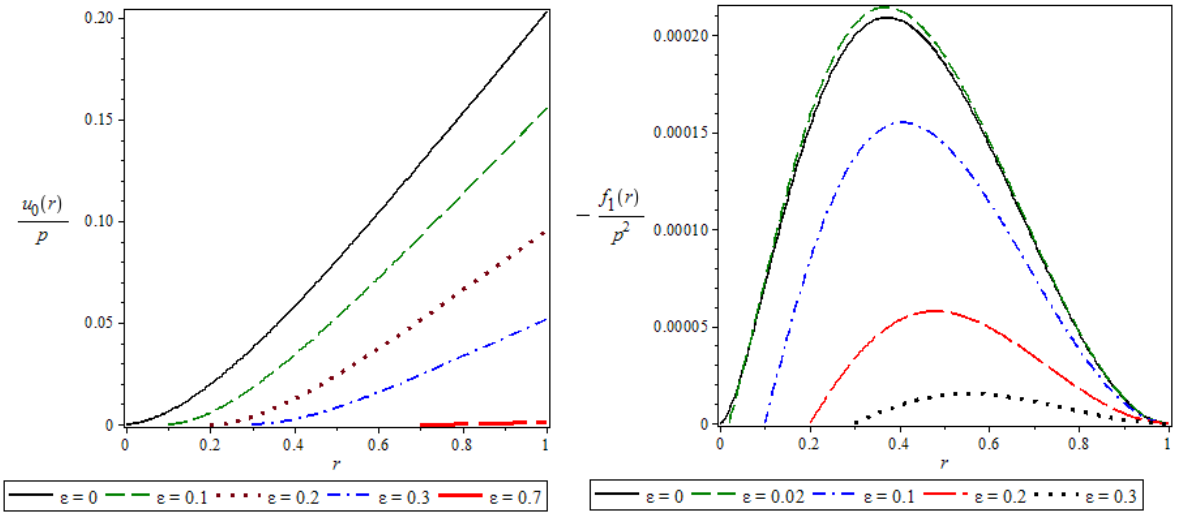

(a) (b)

Figure 5: Plot of the scaled first approximations $u_0(r)$ *and* $f_1(r)$*, where* $\delta \ll 1$ *is a small parameter. We have considered the clamped boundary conditions (9).*

The maximal stress occurs along a circle in the interior of the circular flat plate. Note that we plot $-f_1(r)$ in Figure 5(b), in order to recover the magnitude of the Airy stress function, since $f_1(r) \le 0$. As expected, the stresses are orders of magnitude smaller than the deflections. The qualitative results are very similar to those obtained for the loosely clamped boundary conditions (8), with only minor quantitative differences.

3.3. Comparison of the two plates with free outer edge

For a constant force term $\hat{P}(r) = p$, we can plot the maximal deflection and the maximal value of the Airy stress function as functions dependent on ε. These results are shown in Figure 6. Both quantities are well-defined in the limit $\varepsilon \to 0^+$, which again corresponds to point fixings of negligible radius. The maximal displacement always occurs at the free boundary, so $\max_{\varepsilon<r<1} \frac{u_0(r)}{p} = \frac{u_0(1)}{p}$. However, in contrast to what we saw for the clamped boundary condition solutions, here the maximal displacement is strictly decreasing with ε. As we take the point fixing radius to zero, we find that $\max_{\varepsilon<r<1} \frac{u_0(r)}{p} \to \frac{13}{64}$ as $\varepsilon \to 0^+$, which is exactly what we found in the clamped boundary condition case. Clearly, the loosely clamped boundary conditions permit larger deflections of the plate than do the clamped conditions, for any value of ε satisfying $0 < \varepsilon < 1$. Therefore, in the case of the clamped boundary conditions (9), the maximal value for the out of plane deflection of the thin plate decreases with an increase in ε, which is in contrast to the case for loosely clamped boundary conditions (8).

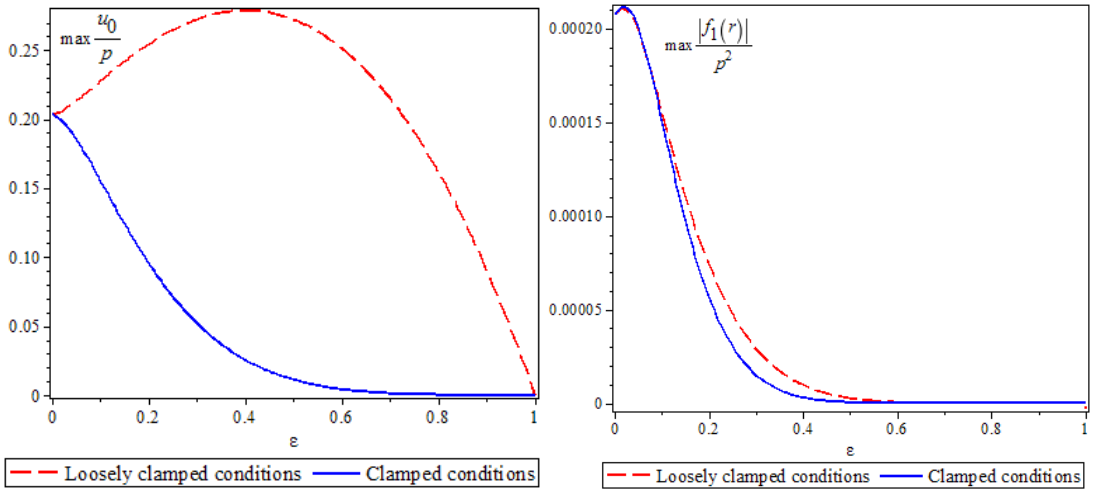

(a) (b)

Figure 6: Plot of the scaled (a) maximal displacement of the plate and (b) Airy stress function, as a function of the point fixing radius $0<\varepsilon<1$. *For comparison we show solutions for the clamped boundary conditions (9) as well as the loosely clamped boundary conditions (8).*

The maximal displacement occurs on the interior of the annular region, so for each fixed $0<\varepsilon<1$, we calculate $\max\limits_{\varepsilon<r<1}\dfrac{|f_1(r)|}{p^2}$. For very small ε, there is an increasing trend in the maximal stress, before the stress function then quickly decreases in maximal magnitude as ε increases. The largest maximal value for the Airy stress function occurs for $\varepsilon\approx 0.02$. This behavior occurs for either of the two boundary conditions. Overall, the loosely clamped conditions result in slightly less stress than do the clamped conditions.

The results show that for point fixings of relatively small radii, say $\varepsilon<0.05$, we have approximately $\max\limits_{\tilde{\varepsilon}^2<x^2+y^2<L^2} w(x,y)\approx 0.2\,p\delta$ and $\max\limits_{\tilde{\varepsilon}^2<x^2+y^2<L^2}|F(x,y)|\approx 2\times10^{-4}\,p^2\delta^2$. Therefore, the displacement displaces a linear scaling with the applied force, while the Airy stress function scales as a quadratic with the applied force. Note that we have

$$\max_{\tilde{\varepsilon}^2<x^2+y^2<L^2}|F(x,y)|\approx 5\times10^{-3}\left(\max_{\tilde{\varepsilon}^2<x^2+y^2<L^2} w(x,y)\right)^2.$$

4. Clamped or loosely clamped outer edge of the plate, free conditions on the inner edge

We shall now direct our attention to the case where the outer edge of the annular plate is held fixed via a clamp or loose clamp, while the inner edge is free. We follow the analytical solution procedure of Section 3.1.

4.1. The annular plate with loosely clamped outer edge, free inner edge

This case corresponds to boundary conditions of the form

$$u''(\varepsilon)=u'''(\varepsilon)=f(\varepsilon)=f'(\varepsilon)=0, \tag{25a}$$

$$u(1)=u''(1)=f(1)=f''(1)=0, \tag{25b}$$

and under a solution of the form (15) involving a particular solution (16), we obtain the parameter values given in Appendix A, equations (A21)-(A24).

Taking the uniform constant force term $\hat{P}(r) = p$, we plot the out of plane deflection for various values of ε in Figure 7. As was true for the previous case, we notice that a variety of behaviors are possible.

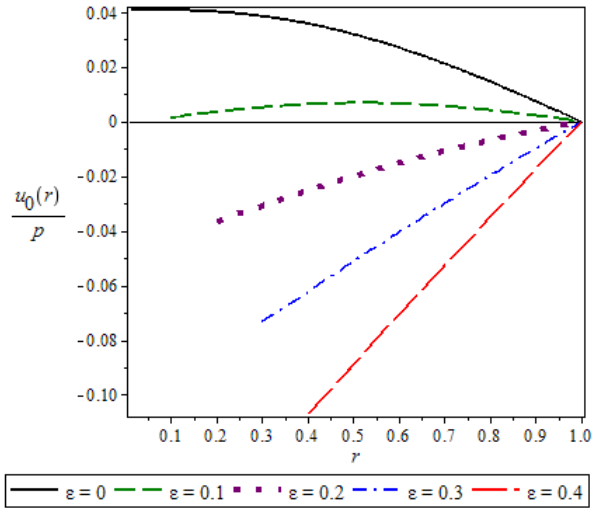

Figure 7: Plot of the scaled first approximation $u_0(r)$ in the expansion (20) under the boundary conditions (25). As a function of ε, the maximal displacement increases, attains a maximal value, and then decreases.

When ε is small enough, namely $0 \le \varepsilon < 0.104$, the deflection will always be in the direction of the applied force, $\hat{P}(r) = p$. When $0.104 < \varepsilon < 0.141$, there will be a region of deflection in the opposite direction of the applied force, located in a center ring adjacent to the interior boundary of the plate. Outside of this ring, the plate bends in the opposite direction, with the deflection out of the plane along the direction of the applied force. Finally, for $0.141 < \varepsilon < 1$, the deflections will always be in the direction opposing the applied force. We conclude, then, that the deflections in this type of plate are more strongly influenced by the form of the boundary conditions, rather than the applied force.

Regarding the Airy stress function, we note that $f_1(r)/p^2$ is at most $O(10^{-4})$ and will decrease as the scaled inner radius ε is increased. The results are not particularly interesting, and we omit the plots for this and future sections as well.

4.2. The annular plate with clamped outer edge, free inner edge

This case corresponds to boundary conditions of the form

$$u''(\varepsilon) = u'''(\varepsilon) = f(\varepsilon) = f'(\varepsilon) = 0, \tag{26a}$$

$$u(1) = u'(1) = f(1) = f''(1) = 0, \tag{26b}$$

and under a solution of the form (15) involving a particular solution (16), we obtain the parameter values given in Appendix A, equations (A29)-(A32).

Taking the uniform force term $\hat{P}(r) = p$, we plot the out of plane deflection $u_0(r)$ for various values of ε in Figure 8. There is great variety in the solution behaviors possible,

depending upon the value of ε.

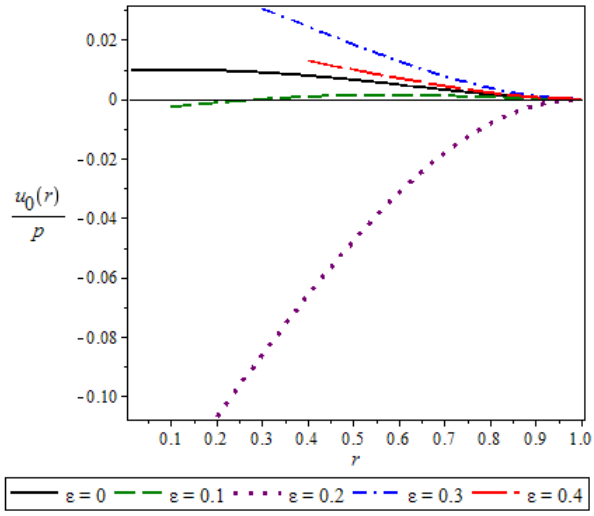

Figure 8: Plot of the scaled first approximation $u_0(r)$ *in the expansions (20) under the boundary conditions (26). As a function of* ε*, the maximal displacement increases, attains a maximal value, and then decreases.*

There is positive deflection of the plate (deflection in the direction of $\hat{P}(r) = p$) when $0 \le \varepsilon < 0.086$. When $0.086 < \varepsilon < 0.141$, the central region of the plate bends opposing the applied force (deflection in the negative direction of the force term) while the outer region of the plate bends in the direction of the applied force. When $0.141 < \varepsilon < 0.2179$, the entire plate is deflected in the opposite direction of the applied force. For most values of the scaled inner radius, $0.2179 < \varepsilon < 1$, the deflection of the plate is completely in the direction of the applied force. In this case, the deflection gradually decreases, with the maximal deflection along the boundary of the inner region in each case. The transition between different plate deflection behaviors for different values of ε is smooth, with one exception: When $\varepsilon \approx 0.218$, there is a bifurcation, with the deflection going from negative to a relatively large positive across the transition. See Appendix B for details on why this bifurcation occurs.

The aforementioned results suggest that the structure of the plate bends in the direction of the applied force when $0 \le \varepsilon < 0.086$ and $\varepsilon^* < \varepsilon < 1$, which is what one typically expects. However, when $0.086 < \varepsilon < \varepsilon^*$, the boundary conditions appear to completely dominate this standard behavior, resulting in some deformations going against the applied force.

While both types of boundary conditions considered in this section result in plates which bend in directions opposing the applied force term for at least some values of the scaled inner radius, there are some differences between the two plates. In the case of a plate with clamped outer conditions and free inner conditions, there exists a discontinuous bifurcation of structure at a fixed critical value of the scaled inner radius. For values larger than this critical value, the plate bends in the direction of the applied force, with `strange' behaviors due to the domination of boundary conditions found only in some intermediate region of scaled inner radius. On the other hand, when considering the plate with loosely clamped conditions, the transition between various types of deformations in the plate appears to be smooth in the parameter ε.

Regarding the Airy stress function for an annular plate with free inner edge and loosely clamped outer edge, we again note that $f_1(r)/p^2$ is at most order $O(10^{-4})$ and will decrease as the scaled inner radius ε is increased. Therefore, the magnitude of the Airy stress function does not differ qualitatively between the two solution types featured in this section.

5. Clamped or loosely clamped condition at each edge of the plate

We now turn our attention to situations where both the inner and outer edge of the annular plate are clamped or loosely clamped. For completeness, we consider and then compare each of the four possibilities. We again follow the perturbation solution procedure of Section 3.1.

5.1. The annular plate with loosely clamped inner edge, loosely clamped outer edge

This case corresponds to boundary conditions of the form

$$u(\varepsilon)=u''(\varepsilon)=f(\varepsilon)=f''(\varepsilon)=0, \tag{27a}$$

$$u(1)=u''(1)=f(1)=f''(1)=0, \tag{27b}$$

and under a solution of the form (15) involving a particular solution (16), we obtain the parameters for (15) listed in (A37)-(A40).

Taking the uniform force term $\hat{P}(r)=p$, we plot the out of plane deflection for various values of ε in Figure 9(a). We find that the deflection of the plate always follows the orientation of the force term $\hat{P}(r)=p$. As ε increases, we have an overall decrease in the maximal deformation extent for large enough ε, although for small ε there is an increase. For fixed ε, the maximal deflection occurs on a circle embedding within the annulus, rather than at either edge. The Airy stress function has maximal magnitude of $O(10^{-5})$ for small ε, and gradually decreases as ε increases toward unity. We omit plots of this function for brevity.

5.2. The annular plate with loosely clamped inner edge, clamped outer edge

This case corresponds to boundary conditions of the form

$$u(\varepsilon)=u''(\varepsilon)=f(\varepsilon)=f''(\varepsilon)=0, \tag{28a}$$

$$u(1)=u'(1)=f(1)=f''(1)=0, \tag{28b}$$

and under a solution of the form (15) involving a particular solution (16), we obtain the parameter values given in (A45)-(A48).

Taking the uniform force term $\hat{P}(r)=p$, we plot the out of plane deflection for various values of ε in Figure 9(b). We find that the deflection of the plate always follows the orientation of the force term $\hat{P}(r)=p$. As ε increases, we have a small increase followed by a decrease in the maximal deformation extent. For fixed ε, the maximal deflection again occurs in a circle within the interior of the annulus. Note that the amplitude of the deformations is much smaller than that for the case where both boundary conditions are loose clamps. The Airy stress function has maximal magnitude of $O(10^{-5})$ for small ε, and gradually decreases as ε increases toward unity.

5.3. The annular plate with clamped inner edge, loosely clamped outer edge

This case corresponds to boundary conditions of the form

$$u(\varepsilon)=u'(\varepsilon)=f(\varepsilon)=f''(\varepsilon)=0, \tag{29a}$$

$$u(1)=u''(1)=f(1)=f''(1)=0, \tag{29b}$$

and under a solution of the form (15) involving a particular solution (16), we the parameter values given in (A53)-(A56).

Taking the uniform force term $\hat{P}(r)=p$, we plot the out of plane deflection for various values of ε in Figure 9(c). Again, we find that the deflection of the plate always follows the orientation of the force term $\hat{P}(r)=p$, and that for fixed ε, the maximal deflection occurs on a circle central to the annulus. As ε increases, we have a uniform decrease in the maximal deformation extent. The Airy stress function has maximal magnitude of $O(10^{-6})$ for small ε, and gradually decreases as ε increases toward unity.

The magnitude of the deflections is again large, akin to what was seen when both edges were loosely clamped. This leads us to believe that the boundary condition at the outer edge most strongly influences the extend of the deformations. On the other hand, and unlike the two previous cases, the deflections decrease uniformly with an increase in ε, while the two previous cases demonstrate a slight increase, followed by a decrease.

5.4. The annular plate with clamped inner edge, clamped outer edge

This case corresponds to boundary conditions of the form

$$u(\varepsilon)=u'(\varepsilon)=f(\varepsilon)=f''(\varepsilon)=0, \tag{30a}$$

$$u(1)=u'(1)=f(1)=f''(1)=0, \tag{30b}$$

and under a solution of the form (15) involving a particular solution (16), we obtain the parameters (A61)-(A64).

Taking the uniform force term $\hat{P}(r)=p$, we plot the out of plane deflection for various values of ε in Figure 9(d). Like the previous examples, we find that the deflection of the plate always follows the orientation of the force term $\hat{P}(r)=p$. For fixed ε, the maximal deflection occurs on a circle central to the annulus. The Airy stress function has maximal magnitude of $O(10^{-6})$ for small ε, and gradually decreases as ε increases toward unity.

As ε increases, we have a uniform decrease in the maximal deformation extent, which agrees with what was seen in Section 5.3. Meanwhile, the deflections are again smaller, more in agreement with what was seen in Section 5.2 than what we observed in Section 5.3. As such, we hypothesize that the clamped outer edge conditions permit much smaller deflections than do the loosely clamped outer edge conditions.

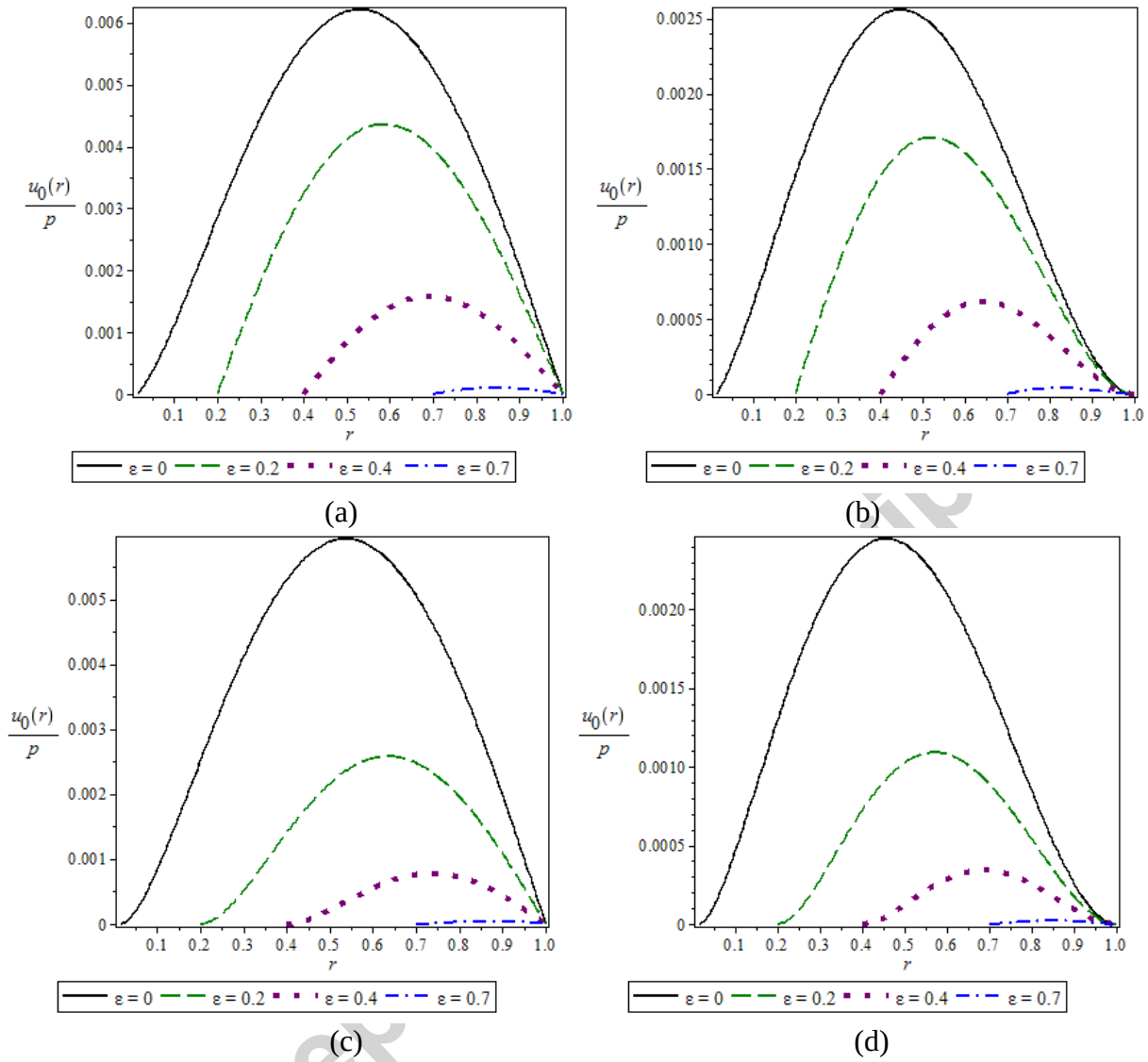

Figure 9: Plot of the scaled first approximation $u_0(r)$ *in the expansion (20) for the deflection of the annular flat plate. We have considered (a) loosely clamped inner and outer boundary conditions (27), (b) loosely clamped inner - clamped outer boundary conditions (28), (c) clamped inner - loosely clamped outer boundary conditions (29), and (d) clamped inner and boundary conditions (30). As a function of* ε*, the maximal displacement increases, attains a maximal value, and then decreases, for all four cases considered.*

5.5. Comparison of the four plates with clamped or loosely clamped edges

For a constant force term $\hat{P}(r) = p$, we can plot the maximal deflection as functions dependent on ε. These results are shown in Figure 10. We see that when the outer edge of the annular plate is loosely clamped, we have the largest deflection away from the plane of the plate. Indeed, the deflections for small ε are more than double those seen when the outer edge boundary condition is that of a clamped edge. This suggests that the size of the deflections can be strongly influenced by the boundary condition on the outer edge of the annular plate.

When the inner edge has a loosely clamped boundary condition, the maximal deflection

occurs at some small positive value of ε. However, when the inner edge has a clamped boundary condition, the maximal deflection occurs when the inner radius ε tends toward zero (corresponding to a circular disk). This suggests that the structure of the deformations is strongly influenced by the boundary condition on the inner edge of the annular plate.

For all cases, note that the deflections observed are much smaller than those for the corresponding annular plates when one of the inner or outer boundaries is free (such as those considered in Sections 3 and 4).

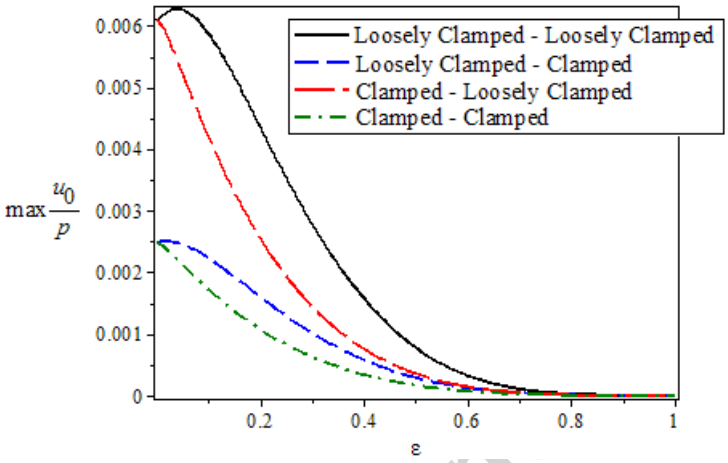

Figure 10: Plot of the maximal scaled displacement of the plate in the case of constant force term, $\max_{\varepsilon<r<1}\frac{u_0(r)}{p} \approx \max_{\varepsilon^2<x^2+y^2<L^2}\frac{w(x,y)}{p\delta}$ *, as a function of the point fixing radius* $0<\varepsilon<1$*. We have compared solutions obtained for the loosely clamped inner and outer boundary conditions (27), loosely clamped inner - clamped outer boundary conditions (28), clamped inner - loosely clamped outer boundary conditions (29), and clamped inner and outer boundary conditions (30).*

6. Discussion

We have obtained analytical and numerical solutions to the Föppl – von Kármán equations governing the deflections of thin, axisymmetric annular plates for various boundary conditions. We saw that the analytical solutions, obtained via a perturbation approach, agreed well with numerical solutions (confer with Figure 4), even for relatively large values of the perturbation parameter, which was taken to be the deflection parameter, δ. This suggests that the scaling obtained in equation (20) is, in fact, the natural scaling for the problem, no matter the size of the deflection parameter. This also suggests that the dominant features of the mathematical problem are the high order linear terms coming from the biharmonic operator and the boundary conditions at both the inner and outer edge. The nonlinear terms, in comparison, were negligible, as comparison with numerical simulations for a range of values of the deflection parameter clearly shows.

In Section 3 we considered the situation where the inner edge of the annular plate was clamped or loosely clamped, while the outer edge was free. This is akin to what happens when point fixings are employed to hold a glass or metal plate in place. For both clamped and loosely clamped inner edge conditions, we note that the plate deformations gradually increased, with maximal deformations occurring at the outer edge. However, plates that were loosely clamped (or, hinged) were shown to permit larger deflections than those plates which were clamped. This

suggests that, if minimizing the extent of deflections under force is desired, one should select clamped edge conditions. As a function of the ratio of inner to outer radius of the annulus, $0<\varepsilon<1$, we observed that as the annulus is made progressively more thin (as ε tends from zero to unity), the clamped plate will have smaller maximal deformation. On the other hand, the maximal deformations of the loosely clamped plate will actually increase for small ε, reaching a maximal value before then decreasing (as shown in Figure 6). Therefore, while the maximal deformation is only slightly different between the two kinds of annular plates when $\varepsilon \sim 0$ or $\varepsilon \sim 1$, when $\varepsilon \sim 0.5$ the difference in maximal deflection extend of the two plates is actually very large, greater than an order of magnitude. In the limit where the annular plates become closed disks ($\varepsilon \to 0$), the maximal deflections are the same. Therefore, it is really in the intermediate regime where very strong differences in maximal deflection are observed.

We considered annular plates which were clamped or loosely clamped on their outer edge, while held free on their inner edge, in Section 4, and these results were far more strange than their counterparts in Section 3. When the outer edge was loosely clamped, the plate deformed in the direction of the applied force when ε was sufficiently small. However, as ε was increased, the solutions underwent a bifurcation, and as the annular plates became more thin, the deflection was in the direction opposing the applied force. What this means is that the mechanics of such plates are dominated by the boundary conditions much more strongly than by the applied force. It is also possible that, while static, such deformations are inherently unstable, and would change in time if temporal effects were included. The case of annular plates with clamped outer conditions and free inner conditions was even more complicated. Again, for small values of ε the deformations will be in the direction of the applied force. For somewhat larger ε, the deformations will become opposite to the direction of the applied force near the interior region and in the direction of the applied force near the exterior of the annulus. As ε is further increased, the solutions undergo a further bifurcation, with all deflections being against the direction of the applied force. There is then a discontinuous bifurcation, at which point a solution does not exist (due to a violation of solvability conditions). For all ε larger than this value at which there is a final bifurcation, the deformation in the plates is uniformly in the direction of the applied force.

In Section 5 we turned our attention to the case where both the inner and outer edges of the plates were clamped or loosely clamped. This case is probably in greatest analogy to the rectangular plate cases present in the literature, in that all boundaries are constrained in some way. In each case, we find that the deformations are in the direction of the applied force. We observe that the choice of boundary condition on the outer edge most strongly influences the size of the deformations, with loosely clamped conditions permitting far larger deformations than clamped conditions, as might be anticipated. The conditions on the inner edge have a much smaller influence, although when one type of condition is fixed for the outer edge, the loosely clamped inner edge plate will exhibit larger deformations than the corresponding plate with clamped inner edge conditions. Furthermore, when the inner edge is clamped, the maximal observed deflection decreases monotonically with the ratio of inner to outer edge radii, ε, while when the inner edge is loosely clamped, the maximal possible deflection occurs for some positive value of ε. These results were summarized graphically in Figure 10.

When comparing the various configurations, we note that the plates considered in Section 3 with the outer edge free have much larger deflections than those plates with both inner and outer edge fixed. This suggests that when applications call for annular plates with at most small deformations under an applied force, one should ensure that both inner and outer edges are

clamped or loosely clamped. On the other hand, point fixings - which operate like the solutions with free outer boundary considered in Section 3 - are of practical importance, and are appropriate if the extent of the deflections is not terribly important. Furthermore, since the solutions scale with the magnitude of the applied force, annular plate solutions fixed only at the inner edge are fine provided that the applied force is sufficiently small. We observe that the Airy stress function is large in magnitude as the extent of the deflection is larger, and therefore the stresses in the plate with only one fixed boundary will tend to be larger than for corresponding plates with two fixed boundaries.

We should note that while the solutions with inner and outer edge fixed exhibit smaller deformations, our results assume that the flat plate will always maintain its structural integrity. Realistically, for large applied force, a plate with both edges fixed might crack or break. Conversely, the plates clamped at the inner edge will exhibit larger deformations from the central plane, yet these plate are more likely to warp or bend toward the vertical than they are to crack or break. Therefore, there may certainly be practical reasons for choosing plates which are only held with central point fixings, even though the Föppl – von Kármán theory does not account for these sorts of behaviors. In contrast to the annular plates studied in Sections 3 and 5, the plates fixed at the outer edge and left free at the inner edge shown in Section 4 were relatively poorly behaved. The plates may bend toward the applied force rather than away from it, and in some cases the plate solutions may not exist (due to violation of a solvability condition). These states might very well be unstable if temporal effects were considered. A stability analysis would determine if such states would be likely to persist in reality. Either way, it seems that the thin annular plates may be poorly behaved if only held fixed on the outer radius, and such configurations may wish to be avoided if one is primarily concerned with ensuring that deflections are small. Of course, the configuration will depend on the precise experiment being performed, so perhaps such boundary conditions permitting more poorly behaved solutions could be useful in studying structural failure. Such pathological failures are likely best understood through time-dependent equations like (2), or more complicated solid mechanics models.

Appendix A: Parameter values used in solutions of the form (15)

The constants in the solution (15) (to equation (7) subject to (8)) are given by a solution to the system

$$\gamma_1\varepsilon^2+\gamma_2+\gamma_3\varepsilon^2\ln(\varepsilon)+\gamma_4\ln(\varepsilon)+U_0(\varepsilon)=0, \tag{A1}$$

$$2\gamma_1+2\gamma_3\ln(\varepsilon)+3\gamma_3-\gamma_4\varepsilon^{-2}+U_0''(\varepsilon)=0, \tag{A2}$$

$$2\gamma_1+3\gamma_3-\gamma_4+U_0''(1)=0, \tag{A3}$$

$$2\gamma_3+2\gamma_4+U_0'''(1)=0. \tag{A4}$$

We find

$$\gamma_1(\varepsilon)=\frac{3U_0'''(1)-2U_0''(1)+\left(8U_0''(\varepsilon)-6U_0''(1)-3U_0'''(1)\right)\varepsilon^2-\left(4U_0''(1)+2U_0'''(1)\right)\varepsilon^2\ln(\varepsilon)}{4\left(1-\varepsilon^2\right)+8\varepsilon^2\ln(\varepsilon)}, \tag{A5}$$

$$\gamma_2(\varepsilon) = -\frac{4U_0(\varepsilon) + \left(3U_0'''(1) - 2U_0''(1) - 4U_0''(\varepsilon)\right)\varepsilon^2 + \left(8U_0''(\varepsilon) - 6U_0''(1) - 3U_0'''(1)\right)\varepsilon^4}{4\left(1-\varepsilon^2\right) + 8\varepsilon^2\ln(\varepsilon)}$$
$$-\frac{4\left(2U_0(\varepsilon) + U_0''(\varepsilon) - U_0''(1) - \frac{1}{2}U_0'''(1)\right)\varepsilon^2\ln(\varepsilon) - 4U_0''(\varepsilon)\varepsilon^4\ln(\varepsilon) - 4U_0'''(1)\varepsilon^2\left(\ln(\varepsilon)\right)^2}{4\left(1-\varepsilon^2\right) + 8\varepsilon^2\ln(\varepsilon)}, \tag{A6}$$

$$\gamma_3(\varepsilon) = -\frac{U_0'''(1) + \left(2U_0''(\varepsilon) - 2U_0''(1) - U_0'''(1)\right)\varepsilon^2}{2\left(1-\varepsilon^2\right) + 4\varepsilon^2\ln(\varepsilon)}, \tag{A7}$$

$$\gamma_4(\varepsilon) = -\frac{\left(U_0''(\varepsilon) - U_0''(1)\right)\varepsilon^2 - U_0'''(1)\varepsilon^2\ln(\varepsilon)}{\left(1-\varepsilon^2\right) + 2\varepsilon^2\ln(\varepsilon)}. \tag{A8}$$

To obtain the solution (15) for equation (7) solved subject to (9), we have the system

$$\gamma_1\varepsilon^2 + \gamma_2 + \gamma_3\varepsilon^2\ln(\varepsilon) + \gamma_4\ln(\varepsilon) + U_0(\varepsilon) = 0, \tag{A9}$$

$$(2\gamma_1 + \gamma_3)\varepsilon + 2\gamma_3\varepsilon\ln(\varepsilon) + \gamma_4\varepsilon^{-1} + U_0'(\varepsilon) = 0, \tag{A10}$$

$$2\gamma_1 + 3\gamma_3 - \gamma_4 + U_0''(1) = 0, \tag{A11}$$

$$2\gamma_3 + 2\gamma_4 + U_0'''(1) = 0. \tag{A12}$$

Solving these four equations to obtain the needed parameters, we find

$$\gamma_1(\varepsilon) = \frac{3U_0'''(1) - 2U_0''(1) - 8U_0'(\varepsilon)\varepsilon + \left(2U_0''(1) + U_0'''(1)\right)\varepsilon^2\left(1 + 2\ln(\varepsilon)\right)}{4\left(1 + 3\varepsilon^2 - 2\varepsilon^2\ln(\varepsilon)\right)}, \tag{A13}$$

$$\gamma_2(\varepsilon) = -\frac{4U_0(\varepsilon) + \left(12U_0(\varepsilon) - 2U_0''(1) + 3U_0'''(1)\right)\varepsilon^2 - 8U_0'(\varepsilon)\varepsilon^3 + \left(2U_0''(1) + U_0'''(1)\right)\varepsilon^4}{4\left(1 + 3\varepsilon^2 - 2\varepsilon^2\ln(\varepsilon)\right)}$$
$$-\frac{\left\{U_0'(\varepsilon)\varepsilon^2 + \left(U_0''(1) - 2U_0(\varepsilon) - \frac{3}{2}U_0'''(1)\right)\varepsilon - U_0'(\varepsilon)\right\}\varepsilon\ln(\varepsilon) + U_0'''(1)\varepsilon^2\left(\ln(\varepsilon)\right)^2}{1 + 3\varepsilon^2 - 2\varepsilon^2\ln(\varepsilon)}, \tag{A14}$$

$$\gamma_3(\varepsilon) = -\frac{U_0'''(1) - 2U_0'(\varepsilon)\varepsilon + \left(2U_0''(1) + U_0'''(1)\right)\varepsilon^2}{2\left(1 + 3\varepsilon^2 - 2\varepsilon^2\ln(\varepsilon)\right)}, \tag{A15}$$

$$\gamma_4(\varepsilon) = -\frac{U_0'(\varepsilon)\varepsilon + \left(U_0'''(1) - U_0''(1)\right)\varepsilon^2 - U_0'''(1)\varepsilon^2\ln(\varepsilon)}{1 + 3\varepsilon^2 - 2\varepsilon^2\ln(\varepsilon)}. \tag{A16}$$

Solving (7) subject to the conditions (25), we obtain the system

$$2\gamma_1+3\gamma_3+2\gamma_3\ln(\varepsilon)-\gamma_4\varepsilon^{-2}+U_0''(\varepsilon)=0, \tag{A17}$$

$$2\gamma_3\varepsilon^{-1}+2\gamma_4\varepsilon^{-3}+U_0'''(\varepsilon)=0, \tag{A18}$$

$$\gamma_1+\gamma_2+U_0(1)=0, \tag{A19}$$

$$2\gamma_1+3\gamma_3-\gamma_4+U_0''(1)=0. \tag{A20}$$

This system can then be solved, resulting in the four parameters

$$\gamma_1(\varepsilon)=\frac{2\left(3+\varepsilon^2\right)U_0''(1)+\varepsilon\left(3\left(1-\varepsilon^2\right)-2\varepsilon^2\ln(\varepsilon)\right)U_0'''(\varepsilon)-4\left(2+\ln(\varepsilon)\right)U_0''(\varepsilon)}{4\left(1-\varepsilon^2+2\ln(\varepsilon)\right)}, \tag{A21}$$

$$\gamma_2(\varepsilon)=\frac{4\left(2+\ln(\varepsilon)\right)U_0''(1)-2\left(3+\varepsilon^2\right)U_0''(\varepsilon)-\varepsilon\left(3\left(1-\varepsilon^2\right)-2\varepsilon^2\ln(\varepsilon)\right)U_0'''(\varepsilon)}{4\left(1-\varepsilon^2+2\ln(\varepsilon)\right)}-U_0(1), \tag{A22}$$

$$\gamma_3(\varepsilon)=\frac{2U_0''(1)-\varepsilon\left(1-\varepsilon^2\right)U_0'''(\varepsilon)-2U_0''(\varepsilon)}{2\left(1-\varepsilon^2+2\ln(\varepsilon)\right)}, \tag{A23}$$

$$\gamma_4(\varepsilon)=\frac{\varepsilon^2\left(U_0''(\varepsilon)-U_0''(1)\right)-\varepsilon^3\ln(\varepsilon)U_0'''(\varepsilon)}{1-\varepsilon^2+2\ln(\varepsilon)}. \tag{A24}$$

Solving (7) subject to the conditions (26), we obtain the system

$$2\gamma_1+3\gamma_3+2\gamma_3\ln(\varepsilon)-\gamma_4\varepsilon^{-2}+U_0''(\varepsilon)=0, \tag{A25}$$

$$2\gamma_3\varepsilon^{-1}+2\gamma_4\varepsilon^{-3}+U_0'''(\varepsilon)=0, \tag{A26}$$

$$\gamma_1+\gamma_2+U_0(1)=0, \tag{A27}$$

$$2\gamma_1+\gamma_3+\gamma_4+U_0'(1)=0. \tag{A28}$$

This system can then be solved, resulting in the four parameters

$$\gamma_1(\varepsilon)=\frac{\varepsilon\left(1+3\varepsilon^2+2\varepsilon^2\ln(\varepsilon)\right)U_0'''(\varepsilon)+2\left(1-\varepsilon^2\right)U_0''(\varepsilon)-4\left(2+\ln(\varepsilon)\right)U_0'(1)}{4\left(3+\varepsilon^2+2\ln(\varepsilon)\right)}, \tag{A29}$$

$$\gamma_2(\varepsilon)=\frac{\left(2+\ln(\varepsilon)\right)U_0'(1)-2\left(1-\varepsilon^2\right)U_0''(\varepsilon)-\varepsilon\left(1+3\varepsilon^2+2\varepsilon^2\ln(\varepsilon)\right)U_0'''(\varepsilon)}{3+\varepsilon^2+2\ln(\varepsilon)}-U_0(1), \tag{A30}$$

$$\gamma_3(\varepsilon)=\frac{2\left(U_0'(1)-U_0''(\varepsilon)\right)-\varepsilon\left(1+\varepsilon^2\right)U_0'''(\varepsilon)}{2\left(3+\varepsilon^2+2\ln(\varepsilon)\right)}, \tag{A31}$$

$$\gamma_4(\varepsilon)=\frac{\varepsilon^2\left(U_0''(\varepsilon)-U_0'(1)\right)-\varepsilon\left(1+\ln(\varepsilon)\right)U_0'''(\varepsilon)}{3+\varepsilon^2+2\ln(\varepsilon)}. \tag{A32}$$

Solving (7) subject to boundary conditions (27), we arrive at the system

$$\gamma_1\varepsilon^2+\gamma_2+\gamma_3\varepsilon^2\ln(\varepsilon)+\gamma_4\ln(\varepsilon)+U_0(\varepsilon)=0, \tag{A33}$$

$$2\gamma_1+2\gamma_3\ln(\varepsilon)+3\gamma_3-\gamma_4\varepsilon^{-2}+U_0''(\varepsilon)=0, \tag{A34}$$

$$\gamma_1+\gamma_2+U_0(1)=0, \tag{A35}$$

$$2\gamma_1+3\gamma_3-\gamma_4+U_0''(1)=0. \tag{A36}$$

This system can then be solved, resulting in the four parameters

$$\gamma_1(\varepsilon)=\frac{\left(3\left(1-\varepsilon^2\right)-2\varepsilon^2\ln(\varepsilon)\right)\left(U_0(\varepsilon)-U_0(1)\right)}{3\left(1-\varepsilon^2\right)^2+4\varepsilon^2\left(\ln(\varepsilon)\right)^2}+\frac{\varepsilon^2\ln(\varepsilon)\left[\left(3+\varepsilon^2\right)U_0''(\varepsilon)-2\left(2+\ln(\varepsilon)\right)U_0''(1)\right]}{3\left(1-\varepsilon^2\right)^2+4\varepsilon^2\left(\ln(\varepsilon)\right)^2}, \tag{A37}$$

$$\gamma_2(\varepsilon)=\frac{\left(3\left(1-\varepsilon^2\right)-2\varepsilon^2\ln(\varepsilon)\right)\left(U_0(1)-U_0(\varepsilon)\right)-4\varepsilon^2\left(\ln(\varepsilon)\right)^2U_0(1)}{3\left(1-\varepsilon^2\right)^2+4\varepsilon^2\left(\ln(\varepsilon)\right)^2}+\frac{\varepsilon^2\ln(\varepsilon)\left[2\left(2+\ln(\varepsilon)\right)U_0''(1)-\left(3+\varepsilon^2\right)U_0''(\varepsilon)\right]}{3\left(1-\varepsilon^2\right)^2+4\varepsilon^2\left(\ln(\varepsilon)\right)^2}, \tag{A38}$$

$$\gamma_3(\varepsilon)=\frac{2\left(1-\varepsilon^2\right)\left(U_0(1)-U_0(\varepsilon)\right)+\varepsilon^2\left(1-\varepsilon^2-2\ln(\varepsilon)\right)U_0''(\varepsilon)-\left(1-\varepsilon^2-2\varepsilon^2\ln(\varepsilon)\right)U_0''(1)}{3\left(1-\varepsilon^2\right)^2+4\varepsilon^2\left(\ln(\varepsilon)\right)^2}, \tag{A39}$$

$$\gamma_4(\varepsilon)=\frac{\varepsilon^2\left[4\ln(\varepsilon)\left(U_0(1)-U_0(\varepsilon)\right)+\left(3-3\varepsilon^2-2\varepsilon^2\ln(\varepsilon)\right)U_0''(\varepsilon)-\left(3-3\varepsilon^2+2\ln(\varepsilon)\right)U_0''(1)\right]}{3\left(1-\varepsilon^2\right)^2+4\varepsilon^2\left(\ln(\varepsilon)\right)^2}. \tag{A40}$$

Solving (7) subject to the boundary conditions (28), we obtain the system

$$\gamma_1\varepsilon^2+\gamma_2+\gamma_3\varepsilon^2\ln(\varepsilon)+\gamma_4\ln(\varepsilon)+U_0(\varepsilon)=0, \tag{A41}$$

$$2\gamma_1+2\gamma_3\ln(\varepsilon)+3\gamma_3-\gamma_4\varepsilon^{-2}+U_0''(\varepsilon)=0, \tag{A42}$$

$$\gamma_1+\gamma_2+U_0(1)=0, \tag{A43}$$

$$2\gamma_1+\gamma_3+\gamma_4+U_0'(1)=0. \tag{A44}$$

This system can then be solved, resulting in the four parameters

$$\gamma_1(\varepsilon)=\frac{\left(1+3\varepsilon^2+2\varepsilon^2\ln(\varepsilon)\right)\left(U_0(\varepsilon)-U_0(1)\right)}{\left(1-\varepsilon^2\right)\left(1+3\varepsilon^2\right)+4\varepsilon^2\ln(\varepsilon)\left(2+\ln(\varepsilon)\right)}$$

$$+\frac{\varepsilon^2\ln(\varepsilon)\left[\left(1-\varepsilon^2\right)U_0''(\varepsilon)-2\left(2+\ln(\varepsilon)\right)U_0'(1)\right]}{\left(1-\varepsilon^2\right)\left(1+3\varepsilon^2\right)+4\varepsilon^2\ln(\varepsilon)\left(2+\ln(\varepsilon)\right)}, \tag{A45}$$

$$\gamma_2(\varepsilon)=\frac{\left(1+3\varepsilon^2+2\varepsilon^2\ln(\varepsilon)\right)\left(\varepsilon^2U_0(1)-U_0(\varepsilon)\right)-4\varepsilon^2\ln(\varepsilon)\left(2+\ln(\varepsilon)\right)U_0(1)}{\left(1-\varepsilon^2\right)\left(1+3\varepsilon^2\right)+4\varepsilon^2\ln(\varepsilon)\left(2+\ln(\varepsilon)\right)}$$
$$+\frac{\varepsilon^2\ln(\varepsilon)\left[2\left(2+\ln(\varepsilon)\right)U_0'(1)-\left(1-\varepsilon^2\right)U_0''(\varepsilon)\right]}{\left(1-\varepsilon^2\right)\left(1+3\varepsilon^2\right)+4\varepsilon^2\ln(\varepsilon)\left(2+\ln(\varepsilon)\right)}, \tag{A46}$$

$$\gamma_3(\varepsilon)=\frac{2\left(1+\varepsilon^2\right)\left(U_0(1)-U_0(\varepsilon)\right)-\varepsilon^2\left(1-\varepsilon^2+2\ln(\varepsilon)\right)U_0''(\varepsilon)-\left(1-\varepsilon^2-2\varepsilon^2\ln(\varepsilon)\right)U_0'(1)}{\left(1-\varepsilon^2\right)\left(1+3\varepsilon^2\right)+4\varepsilon^2\ln(\varepsilon)\left(2+\ln(\varepsilon)\right)}, \tag{A47}$$

$$\gamma_4(\varepsilon)=\frac{4\varepsilon^2\left(1+\ln(\varepsilon)\right)\left(U_0(\varepsilon)-U_0(1)\right)}{\left(1-\varepsilon^2\right)\left(1+3\varepsilon^2\right)+4\varepsilon^2\ln(\varepsilon)\left(2+\ln(\varepsilon)\right)}$$
$$+\frac{\varepsilon^2\left[\left(1-\varepsilon^2+2\varepsilon^2\ln(\varepsilon)\right)U_0''(\varepsilon)-\left(3-3\varepsilon^2+2\ln(\varepsilon)\right)U_0'(1)\right]}{\left(1-\varepsilon^2\right)\left(1+3\varepsilon^2\right)+4\varepsilon^2\ln(\varepsilon)\left(2+\ln(\varepsilon)\right)}. \tag{A48}$$

Solving (7) subject to the boundary conditions (29), we obtain the system

$$\gamma_1\varepsilon^2+\gamma_2+\gamma_3\varepsilon^2\ln(\varepsilon)+\gamma_4\ln(\varepsilon)+U_0(\varepsilon)=0, \tag{A49}$$

$$\left(2\gamma_1+\gamma_3\right)\varepsilon+2\gamma_3\varepsilon\ln(\varepsilon)+\gamma_4\varepsilon^{-1}+U_0'(\varepsilon)=0, \tag{A50}$$

$$\gamma_1+\gamma_2+U_0(1)=0, \tag{A51}$$

$$2\gamma_1+3\gamma_3-\gamma_4+U_0''(1)=0. \tag{A52}$$

This system can then be solved, resulting in the four parameters

$$\gamma_1(\varepsilon)=\frac{\left(3+\varepsilon^2+2\varepsilon^2\ln(\varepsilon)\right)\left(U_0(\varepsilon)-U_0(1)\right)}{\left(1-\varepsilon^2\right)\left(3+\varepsilon^2\right)+4\varepsilon^2\ln(\varepsilon)\left(2-\ln(\varepsilon)\right)}$$
$$+\frac{2\varepsilon^2\left(\ln(\varepsilon)\right)^2U_0''(1)-\varepsilon\left(3+\varepsilon^2\right)\ln(\varepsilon)U_0'(\varepsilon)}{\left(1-\varepsilon^2\right)\left(3+\varepsilon^2\right)+4\varepsilon^2\ln(\varepsilon)\left(2-\ln(\varepsilon)\right)}, \tag{A53}$$

$$\gamma_2(\varepsilon)=\frac{\varepsilon^2\left(3+\varepsilon^2-6\ln(\varepsilon)+4\left(\ln(\varepsilon)\right)^2\right)U_0(1)-\left(3+\varepsilon^2+2\varepsilon^2\ln(\varepsilon)\right)U_0(\varepsilon)}{\left(1-\varepsilon^2\right)\left(3+\varepsilon^2\right)+4\varepsilon^2\ln(\varepsilon)\left(2-\ln(\varepsilon)\right)}, \tag{A54}$$

$$\gamma_3(\varepsilon)=\frac{2\left(1+\varepsilon^2\right)\left(U_0(1)-U_0(\varepsilon)\right)+\varepsilon\left(1-\varepsilon^2-2\ln(\varepsilon)\right)U_0'(\varepsilon)-\left(1-\varepsilon^2-2\varepsilon^2\ln(\varepsilon)\right)U_0''(1)}{\left(1-\varepsilon^2\right)\left(3+\varepsilon^2\right)+4\varepsilon^2\ln(\varepsilon)\left(2-\ln(\varepsilon)\right)}, \tag{A55}$$

$$\gamma_4(\varepsilon)=\frac{4\varepsilon^2\left(1-\ln(\varepsilon)\right)\left(U_0(1)-U_0(\varepsilon)\right)}{\left(1-\varepsilon^2\right)\left(3+\varepsilon^2\right)+4\varepsilon^2\ln(\varepsilon)\left(2-\ln(\varepsilon)\right)}$$
$$-\frac{\varepsilon^2\left[\left(3-3\varepsilon^2+2\varepsilon^2\ln(\varepsilon)\right)U_0'(\varepsilon)+\left(1-\varepsilon^2+2\ln(\varepsilon)\right)U_0''(1)\right]}{\left(1-\varepsilon^2\right)\left(3+\varepsilon^2\right)+4\varepsilon^2\ln(\varepsilon)\left(2-\ln(\varepsilon)\right)}. \quad \text{(A56)}$$

Solving (7) subject to the boundary conditions (30), we obtain the system

$$\gamma_1\varepsilon^2+\gamma_2+\gamma_3\varepsilon^2\ln(\varepsilon)+\gamma_4\ln(\varepsilon)+U_0(\varepsilon)=0, \quad \text{(A57)}$$

$$\left(2\gamma_1+\gamma_3\right)\varepsilon+2\gamma_3\varepsilon\ln(\varepsilon)+\gamma_4\varepsilon^{-1}+U_0'(\varepsilon)=0, \quad \text{(A58)}$$

$$\gamma_1+\gamma_2+U_0(1)=0, \quad \text{(A59)}$$

$$2\gamma_1+\gamma_3+\gamma_4+U_0'(1)=0. \quad \text{(A60)}$$

This system can then be solved, resulting in the four parameters

$$\gamma_1(\varepsilon)=\frac{\left(1-\varepsilon^2-2\varepsilon^2\ln(\varepsilon)\right)\left(U_0(\varepsilon)-U_0(1)\right)-\varepsilon\left(1-\varepsilon^2\right)\ln(\varepsilon)U_0'(\varepsilon)+2\varepsilon^2\left(\ln(\varepsilon)\right)^2U_0'(1)}{\left(1-\varepsilon^2\right)^2-4\varepsilon^2\left(\ln(\varepsilon)\right)^2}, \quad \text{(A61)}$$

$$\gamma_2(\varepsilon)=\frac{\varepsilon^2\left(1-\varepsilon^2-2\varepsilon^2\ln(\varepsilon)-4\varepsilon^2\left(\ln(\varepsilon)\right)^2\right)U_0(1)-\left(1-\varepsilon^2-2\varepsilon^2\ln(\varepsilon)\right)U_0(\varepsilon)}{\left(1-\varepsilon^2\right)^2-4\varepsilon^2\left(\ln(\varepsilon)\right)^2}$$
$$+\frac{\varepsilon\left(1-\varepsilon^2\right)\ln(\varepsilon)U_0'(\varepsilon)-2\varepsilon^2\left(\ln(\varepsilon)\right)^2U_0'(1)}{\left(1-\varepsilon^2\right)^2-4\varepsilon^2\left(\ln(\varepsilon)\right)^2}, \quad \text{(A62)}$$

$$\gamma_3(\varepsilon)=\frac{2\left(1-\varepsilon^2\right)\left(U_0(1)-U_0(\varepsilon)\right)+\varepsilon\left(1-\varepsilon^2+2\ln(\varepsilon)\right)U_0'(\varepsilon)-\left(1-\varepsilon^2+2\varepsilon^2\ln(\varepsilon)\right)U_0'(1)}{\left(1-\varepsilon^2\right)^2-4\varepsilon^2\left(\ln(\varepsilon)\right)^2}, \quad \text{(A63)}$$

$$\gamma_4(\varepsilon)=\frac{4\varepsilon^2\ln(\varepsilon)\left(U_0(\varepsilon)-U_0(1)\right)\varepsilon^2\left(1-\varepsilon^2+2\ln(\varepsilon)\right)U_0'(1)-\varepsilon\left(1-\varepsilon^2+2\varepsilon^2\ln(\varepsilon)\right)U_0'(\varepsilon)}{\left(1-\varepsilon^2\right)^2-4\varepsilon^2\left(\ln(\varepsilon)\right)^2}. \quad \text{(A64)}$$

Appendix B: Bifurcation in the solution with parameters (A25)-(A28)

As noted in our discussion of the solutions, there is a discontinuous bifurcation at $\varepsilon\approx 0.2179$ which serves to partition the various regions in a rather fundamental way, since it prevents smooth deformations between small and large ε behaviors. In order to better understand the reason why we have such a bifurcation for this case, yet not in any of the other cases considered, observe that each term in (A25)-(A28) involves a factor of the form $\left(3+\varepsilon^2+2\ln(\varepsilon)\right)^{-1}$. Observe that $3+\varepsilon^2+2\ln(\varepsilon)$ is a continuous function for $0<\varepsilon<1$, is negative as $\varepsilon\to 0$, and is positive as $\varepsilon\to 1$. Therefore, there must exist some $\varepsilon^*\in(0,1)$ for

which $3+\left(\varepsilon^*\right)^2+2\ln\left(\varepsilon^*\right)=0$. We find that there is a unique root on the unit interval, which is given by

$$\varepsilon^*=\exp\left(-\frac{3}{2}-\frac{1}{2}\,\mathrm{LambertW}\left(e^{-3}\right)\right)\approx 0.2179, \tag{B1}$$

as anticipated. (Here, LambertW denotes the Lambert W function; for discussion see, e.g., [62].) Since $\left(3+\varepsilon^2+2\ln\left(\varepsilon\right)\right)^{-1}\to\pm\infty$ as $\varepsilon\to\varepsilon^*$, the solution defined by (A25)-(A28) becomes degenerate as $\varepsilon\to\varepsilon^*$. This is the cause of the bifurcation observed in Figure 8. When $\varepsilon=\varepsilon^*$, the solutions using the parameters (A25)-(A28) are no longer valid. This is the only such case of a degeneracy found in this paper.

To better understand why this bifurcation of solutions occurs, let us recast the system (A21)-(A24) as the matrix system

$$\begin{bmatrix} 2 & 0 & 3+2\ln\left(\varepsilon\right) & -\varepsilon^{-2} \\ 0 & 0 & 2\varepsilon^{-1} & 2\varepsilon^{-3} \\ 1 & 1 & 0 & 0 \\ 2 & 0 & 1 & 1 \end{bmatrix}\begin{bmatrix} \gamma_1 \\ \gamma_2 \\ \gamma_3 \\ \gamma_4 \end{bmatrix}=\begin{bmatrix} U_0''\left(\varepsilon\right) \\ U_0'''\left(\varepsilon\right) \\ U_0\left(1\right) \\ U_0'\left(1\right) \end{bmatrix}. \tag{B2}$$

The solvability condition for the radial biharmonic equation subject to the boundary conditions (26) is therefore given by

$$0\neq\det\begin{bmatrix} 2 & 0 & 3+2\ln\left(\varepsilon\right) & -\varepsilon^{-2} \\ 0 & 0 & 2\varepsilon^{-1} & 2\varepsilon^{-3} \\ 1 & 1 & 0 & 0 \\ 2 & 0 & 1 & 1 \end{bmatrix}=-4\varepsilon^{-3}\left(3+\varepsilon^2+2\ln\left(\varepsilon\right)\right). \tag{B3}$$

At $\varepsilon=\varepsilon^*$, the determinant vanishes, and hence the solvability condition is not met. Therefore, solutions to the radial biharmonic equation for the boundary conditions (26) exist only for $0<\varepsilon<\varepsilon^*$ or $\varepsilon^*<\varepsilon<1$. For all other cases considered in this paper, one may verify that the relevant form of the solvability condition is satisfied for all $0<\varepsilon<1$, and hence the present case is rather unique in having such poor behavior.

References

[1] A. Föppl, Vorlesungen über technische Mechanik, B.G. Teubner, Bd. 5., p. 132, Leipzig, Germany (1907)
[2] T. von Kármán, Festigkeitsproblem im Maschinenbau, Encyk. D. Math. Wiss. IV, 311–385 (1910)
[3] E. Cerda and L. Mahadevan, Geometry and Physics of Wrinkling, Phys. Rev. Lett. 90 (2003) 074302.
[4] L. D. Landau and E. M. Lifshitz, "Theory of Elasticity". (3rd ed. ISBN 075062633X)
[5] J. Awrejcewicz, V. A. Krysko, and A. V. Krysko, Complex parametric vibrations of flexible rectangular plates, Meccanica 39(3) (2004) 221-244.

[6] J. Awrejcewicz, V. A. Krysko, and T. Moldenkova, Mathematical model of dissipative parametric vibrations of flexible plates with non-homogeneous boundary conditions, Mathematical Problems in Engineering 2006 (2006) 85623.
[7] V. A. Krysko, J. Awrejcewicz, and T. Molodenkova, A mathematical model for non-linear dynamics of conservative systems with non-homogeneous boundary conditions, Computers & Structures 84(29) (2006) 1918-1924.
[8] A.V. Krysko, J. Awrejcewicz, S. P. Pavlov, M. V. Zhigalov, and V. A. Krysko, On the iterative methods of linearization, decrease of order and dimension of the Karman-type PDEs, The Scientific World Journal 2014 (2014) 792829.
[9] J. Awrejcewicz, J., V. A. Krysko, and I. V. Kravtsova, Dynamics and statics of flexible axially-symmetric shallow shells, Mathematical Problems in Engineering 2006 (2006) 35672.
[10] J. Awrejcewicz and V. A. Krysko, Chaos in Structural Mechanics, Springer, Berlin, 2008.
[11] X. Chen and J. W. Hutchinson, Herringbone buckling patterns of compressed thin films on compliant substrates, ASME Journal of Applied Mechanics 71 (2004) 597-603.
[12] Z.Y. Huang, W. Hong, Z. Suo, Nonlinear analyses of wrinkles in a film bonded to a compliant substrate, Journal of the Mechanics and Physics of Solids 53 (2005) 2101-2118.
[13] B. Audoly, Mode-dependent toughness and the delamination of compressed thin films, Journal of the Mechanics and Physics of Solids 48 (2000) 2101-2118.
[14] J.W. Hutchinson and Z. Suo, Mixed-mode cracking in layered materials, Advances in Applied Mechanics 29 (1992) 63-191.
[15] J.-S. Wang and A. G. Evans, Measurement and analysis of buckling and buckle propagation in compressed oxide layers on superalloy substrates, Acta Materialia 46 (1998) 4993-5005.
[16] M.W. Moon, K.R. Lee, K.H. Oh and J.W. Hutchinson, Buckle delamination on patterned substrates, Acta Materialia 52 (2004) 3151-3159.
[17] B. Audoly and A. Boudaoud, Buckling of a stiff film bound to a compliant substrate—Part I: Formulation, linear stability of cylindrical patterns, secondary bifurcations, Journal of the Mechanics and Physics of Solids 56 (2008) 2401-2421.
[18] B. Audoly and A. Boudaoud, Buckling of a stiff film bound to a compliant substrate—Part II: A global scenario for the formation of herringbone pattern, Journal of the Mechanics and Physics of Solids 56 (2008) 2422-2443.
[19] G.H. Knightly, An existence theorem for the von Kármán equations, Archive for Rational Mechanics and Analysis 27 (1969) 233-242.
[20] A. Boudaoud, P. Patrício, Y. Couder and M. Ben Amar, Dynamics of singularities in a constrained elastic plate, Nature 407 (2000) 718-720.
[21] E. Cerda and L. Mahadevan, Geometry and Physics of Wrinkling, Phys. Rev. Lett. 90 (2003) 074302.
[22] H. Ben Belgacem, S. Conti, A. DeSimone and S. Müller, Rigorous Bounds for the Föppl—von Kármán Theory of Isotropically Compressed Plates, Journal of Nonlinear Science 10 (2000) 661-683.
[23] T. Mora and A. Boudaoud, Buckling of swelling gels, The European Physical Journal E 20 (2006) 119-124.
[24] T. Mora and A. Boudaoud, Thin elastic plates: On the core of developable cones, Europhysics Letters 59 (2002) 41-47.
[25] N. Uchida, Orientational order in buckling elastic membranes, Physica D: Nonlinear Phenomena 205 (2005) 267-274.
[26] W. Jin and P. Sternberg, Energy estimates for the von Kármán model of thin-film blistering, Journal of Mathematical Physics 42 (2001) 192.
[27] R. A. Van Gorder, Analytical method for the construction of solutions to the Föppl – von Kármán equations governing deflections of a thin plate, International Journal of Non-Linear Mechanics 47 (2012) 1-6.
[28] J. Awrejcewicz, V. A. Krysko, A. V. Krysko, Spatio-temporal chaos and solitons exhibited by von

Kármán model, International Journal of Bifurcation and Chaos 12 (2002) 1465-1513.
[29] M. Lewicka, L. Mahadevan, M. R. Pakzad, The Föppl – von Kármán equations for plates with incompatible strains, Proceedings of the Royal Society A 467 (2011) 402-426.
[30] J. Awrejcewicz, I. V. Andrianov, V. V. Danishevs'kyy, and A. O. Ivankov, Asymptotic Methods in the Theory of Plates with Mixed Boundary Conditions, Wiley, 2014.
[31] S. Way, Bending of circular plate with large deflection, ASME Trans. Appl. Mech. 56 (1934) 627–636.
[32] J. J. Vincent, The bending of a thin circular plate, Phil. Mag. 12 (1931) 185–196.
[33] Chien Wei-Zang, Large deflection of a circular clamped plate under uniform pressure, Chinese J. Phys. 7 (1947) 102–113
[34] J. P. Frakes and J. G. Simmonds, Asymptotic Solutions of the Von Karman Equations for a Circular Plate Under a Concentrated Load, Journal of Applied Mechanics 52 (1985) 326-330.
[35] Y. Kai-Yuan, Z. Xiao-Jing, and Z. You-He, An analytical formula of the exact solution to von Kármán's equations of a circular plate under a concentrated load, International Journal of Non-linear Mechanics 24 (1989) 551-560.
[36] L. A. Taber, Asymptotic expansions for large elastic strain of a circular plate, International Journal of Solids and Structures 23 (1987) 719-731.
[37] I. Tadjbakhsh and E. Saibel, On the Large Elastic Deflections of Plates, ZAMM-Zeitschrift für Angewandte Mathematik und Mechanik 40(5-6) (1960) 259-268.
[38] V. G. Hart and D. J. Evans, Non-linear Bending of an Annular Plate by Transverse Edge Forces, Journal of Mathematics and Physics 43 (1964) 275-303.
[39] D. J. Evans and V. G. Hart, On a system of simplified equations for finite axisymmetric deflections of an annular plate, Journal of Mathematics and Physics 45 (1966) 367-369.
[40] J. T. Tielking, Axisymmetric Banding of Annular Plates, Journal of Applied Mechanics 45 (1978) 834-838.
[41] J. T. Tielking, Asymmetric bending of annular plates, International Journal of Solids and Structures 16 (1980) 361-373.
[42] J. N. Reddy and C. L. Haung, Nonlinear axisymmetric bending of annular plates with varying thickness, International Journal of Solids and Structures 17 (1981) 811-825.
[43] V. G. Hart and F. Holland, Existence and uniqueness problems for an elastic annular plate at large transverse deflections, Proc. R. Ir. Acad. 86(2) (1986) 95-106.
[44] H. B. Thompson, Existence and Uniqueness Problems for an Elastic Annular Plate, Proc. R. Ir. Acad. 88(1) (1988) 61-70.
[45] R. H. Plaut, Linearly elastic annular and circular membranes under radial, transverse, and torsional loading. Part I: large unwrinkled axisymmetric deformations, Acta Mechanica 202 (2009) 79-99.
[46] Z. Liu, W. Hong, Z. Suo, S. Swaddiwudhipong, and Y. Zhang, Modeling and simulation of buckling of polymeric membrane thin film gel, Computational Materials Science 49 (2010) S60-S64.
[47] D. K. Marker and C. H. Jenkins, Surface precision of optical membranes with curvature, Optics Express 1 (1997) 324-331.
[48] Z. Liu, S. Swaddiwudhipong, and W. Hong, Pattern formation in plants via instability theory of hydrogels, Soft Matter 9 (2013) 577-587.
[49] R. H. Plaut, Linearly elastic annular and circular membranes under radial, transverse, and torsional loading. Part II: Vibrations about deformed equilibria, Acta Mechanica 202 (2009) 101-110.
[50] P. C. Dumir, Nonlinear vibration and postbuckling of orthotropic thin annular plates, Composite Structures 5 (1986) 61-77.
[51] P. Cobelli, P. Petitjeans, A. Maurel, V. Pagneux, and N. Mordant, Space-time resolved wave turbulence in a vibrating plate, Physical Review Letters 103 (2009) 204301.
[52] J. Tani, Elastic instability of a heated annular plate under lateral pressure, Journal of Applied Mechanics 48 (1981) 399-403.
[53] M. Schwarzbart and A. Steindl, Buckling of a non-Euclidean annular plate, PAMM 11 (2011) 277-278.

[54] B. Davidovitch, R. D. Schroll, D. Vella, M. Adda-Bedia, and E. A. Cerda, Prototypical model for tensional wrinkling in thin sheets, Proceedings of the National Academy of Sciences 108(45) (2011) 18227-18232.
[55] C. D. Coman and X. Liu, Buckling-resistant thin annular plates in tension, Mathematics and Mechanics of Solids 19 (2014) 925-951.
[56] C. D. Coman, Some applications of the WKB method to the wrinkling of bi-annular plates in tension, Acta Mechanica 224 (2013) 399-423.
[57] J. Williams, Indentation of a floating film: the role of elasticity and incompressibility. Master's Dissertation. University of Oxford, Oxford, UK (2015).
[58] F. Bernard and L. Daudeville, Point fixings in annealed and tempered glass structures: Modeling and optimization of bolted connections, Engineering structures 31 (2009) 946-955.
[59] M. A. Vyzantiadou and A. V. Avdelas, Point fixed glazing systems: technological and morphological aspects, Journal of Constructional Steel Research 60 (2004) 1227-1240.
[60] C. O. Rex and W. S. Easterling, Behavior and modeling of a bolt bearing on a single plate, Journal of Structural Engineering 129 (2003) 792-800.
[61] D. Duerr, Pinned connection strength and behavior, Journal of Structural Engineering 132 (2006) 182-194.
[62] R. M. Corless, G. H. Gonnet, D. E. G. Hare, D. J. Jeffrey, D. E. Knuth, On the Lambert W function, Advances in Computational Mathematics 5 (1996) 329–359.

Highlights

Deformations of flat annular plates studied under Föppl – von Kármán equations

Asymptotic solutions obtained for various boundary condition configurations

Ratio of the inner to outer radius will strongly influence the properties of the solutions

Boundary conditions can be selected to control plate deformations